s

Molecular scale description of interfacial mass transfer in phase separated aqueous secondary organic aerosol

Mária Lbadaoui-Darvas[1], Satoshi Takahama[1], and Athanasios Nenes[1,2]

[1]School of Architecture, Civil and Environmetal Engineering, Swiss Federal Institute of Technology, Lausanne, 1015, Switzerland
[2]Institute of Chemical Engineering Sciences, Foundation for Research and Technology Hellas, Patras, Greece GR-26504

Correspondence: NAME (EMAIL)

Abstract. TEXT

Contents

1 Introduction

Aerosol-cloud interactions constitute one of the most important sources of uncertainty in assessments of anthropogenic climate change. (IPCC) The number, size and composition characteristics of aerosol influence the number of droplets that can form in cloudy updrafts, which in turn affect the microphysical evolution and radiative properties in a complex and intricate way up to the climate scale. Cloud droplets form upon a subset of the available particles, called cloud condensation nuclei (CCN), that reach a state of unstable equilibrium with the surrounding supersaturated water vapor that develops in a cloudy updraft, and subsequently experience unconstrained growth. The dynamics of water uptake on CCN is a critical process that influences the level of supersaturation that can develop in clouds (Raatikainen et al., 2013) and is affected by the interplay of gas phase diffusion, interfacial mass transfer and diffusion in the particle phase. Gas phase diffusion determines condensation rates when the mean free path of gas phase molecules is lower than the particle size. Particle phase diffusion is rate limiting in glassy and semisolid aerosol, while interfacial mass transfer is important when particle size is comparable to the mean free path of molecules in the vapor phase.

Limitations on condensational particle growth by interfacial mass transfer are quantified by the mass accommodation coefficient (α), which is the ratio of molecules absorbed by the particle and the total number of molecules colliding with the surface. While widely used to describe gas-to-particle partitioning in atmospheric systems, the concept of the mass accommodation coefficient is not unambigously defined. Firstly, a clear definition of the reference state – i.e. that state beyond which a water molecules is considered to have partitioned to the particle phase – is unclear. The most commonly accepted definition of α uses adsorption at the particle surface or absorption by the first few molecular layers of the particle as a reference state, while a

penetration depth dependent definition(Shiraiwa and Pöschl, 2020) have also been proposed. Equally importantly, the temperature dependent trends in α, whose magnitude and direction is strongly system specific(Li et al., 2001; Davidovits et al., 2004; Zientara et al., 2008; Davies et al., 2013; Roy et al., 2020), are typically not accounted for by parcel models of cloudy updrafts, which tend use a single α value to simulate the entire range on which the temperature of a rising air parcel varies.(Morales Betancourt and Nenes, 2014) This can potentially lead to systematic errors in predictions, whose magnitude varies with elevation. Ambiguities surrounding the process of gas-to-particle partitioning are deeply rooted in its dependence on the molecular scale mechanism of gas-to-particle partitioning which varies as a function of particle structure and composition, and which has been mapped only for a handful of systems. $\alpha \sim 1$ for particles whose surface is composed of dominantly water (Clement et al., 1996; Morita et al., 2004; Voigtländer et al., 2007), while α can be very reduced for hydrophobic surfaces. For long chained alcohol model films α was found to be as low as $10^{-3} - 10^{-5}$ from molecular dynamics (Takahama and Russell, 2011; Ergin and Takahama, 2016; Johansson et al., 2020) and experimental studies. (Diveky et al., 2019; Johansson et al., 2020). Gas-to-particle partitioning on secondary organic aerosol (SOA), which constitutes a significant fraction of the total particulate matter on a global scale(Fuzzi et al., 2006), is usually characterized by $\alpha > 0.1$.(**??**)

Modeling studies have long shown that reduced mass accommodations coefficients result in increased droplet number concentration in clouds, owing to the slow condensation of water vapor in the initial stages of cloud formation, which in turn elevates supersaturation and allows for more CCN to activate. For these kinetic delays to be important for climate simulations, the update coefficient needs to be less than 0.1 (Raatikainen et al., 2013). To date, although low values of α values have been reported for select systems, analysis of droplet formation upon aerosol from a broad range of environments - even aerosol with large amounts of hydrophobic material (Moore et al., 2012; Raatikainen et al., 2013) has not indicated uptake coefficients below 0.1. Molecular simulations also suggest this is unlikely to be the level. (Miles et al., 2012; Johansson et al., 2020; von Domaros et al., 2020)

Typical values of $\alpha > 0.1$ observed in SOA suggest that they alter CCN activity only to a negligible extent due to kinetic delays in gas-to-particle partitioning. Nevertheless, increased CCN activity compared to the one predicted by the κ-Köhler theory has been reported for SOA in particular for liquid-liquid phase separated particles.(Prenni et al., 2007; Pajunoja et al., 2015; Liu et al., 2018) Liquid-liquid phase separation (LLPS) occurs in deliquesced aerosol rich in SOA if the O:C ratio of the organics is lower than 0.8. (Song et al., 2012, 2017; Renbaum-Wolff et al., 2016) Particles formed by LLPS have either core-shell or partially engulfed morphopolies.() LLPS organic shells are non-ideal mixed multilayers, potentially affecting interfacial mass transfer kinetics in a complex way which cannot be interpreted via the concept of a single mass accommodation coefficient. (Krieger et al., 2012; Davies et al., 2013) Increased CCN activity of LLPS particles may be due to i) reduced surface tension due to the high concentrations organic molecules at the surface of LLPS particles ; ii) surface adsorption (Pajunoja et al., 2015; Sareen et al., 2013) or iii) non-ideal mixing. Surface tension reduction is proven in laboratory (Song et al., 2012, 2017; Renbaum-Wolff et al., 2016) and field experiments (Facchini et al., 1999), and its role in enhancing CCN activity has been extensively discussed.(Ruehl et al., 2012, 2016; Noziere, 2016; Ovadnevaite et al., 2017) The existence of a long-lived surface adsorbed states is unlikely when the outer phase has randomly oriented hydrophobic groups, due to the rapid formation of H-bonds seen in MD simulations (Johansson et al., 2020), and was recently proved to be insignificant also by experiments.

(Liu et al., 2018) Recent studies point out the importance of non-ideal mixing in reduced CCN activity by introducing a Flory-Huggins type of treatment in a κ-Köhler model. (Liu et al., 2018) The connection between the above mentioned three contributions, however, has yet to be established.

Both the ambiguities surrounding the definition of gas-to-particle partitioning in non-well mixed compounds, and the lack of detailed understanding of the effect of LLPS on cloud droplet growth and activation are closely tied to our limited knowledge about the molecular scale mechanism of the partitioning process. Timescales associated with interfacial mass transfer of a single water molecule to an aerosol particle are conveniently studied by molecular dynamics (MD) simulations, using either direct impinging (Vieceli et al., 2005; Bahadur and Russell, 2008; Takahama and Russell, 2011; Johansson et al., 2020) or umbrella sampling techniques (Ergin and Takahama, 2016). Molecular dynamics simulations have provided evidence for near unity surface accommodation coefficients on pure water surfaces (Morita et al., 2004; Vieceli et al., 2005; Takahama and Russell, 2011) and reproduced very reduced ones characteristic of hydrophobic surfaces. (Ergin and Takahama, 2016; Miles et al., 2016; Johansson et al., 2020) In direct impinging simulations, gas-phase molecules are launched with an initial velocity towards the bulk phase in several trials and the mass accommodation coefficient is simply estimated as the ratio of successful trials. It is however, prone to misidentify molecules that are adsorbed at the surface but desorbed later without entering the bulk liquid phase as false positives. Umbrella sampling simulations are used to reconstruct the free energy profile of water uptake from a series equilibrium simulations with the position of the gas phase molecule at different distances from the bulk, which is then converted to mass accommodation coefficient using the transition state theory.(Ergin and Takahama, 2016) As a typical quasi equilibrium method, umbrella sampling neglects the effect of friction, which is very important in such fast processes. A very recent study used well tempered metadynamics to estimate equilibrium partitioning coefficients of volatile organics.(von Domaros et al., 2020) In this work an alternative approach based on steered molecular dynamics (Steered MD) (Park and Schulten, 2004) is proposed. It has been successful at exploring free energy profiles along distance-related reaction coordinates in biophysical contexts,(e.g.: (Allen et al., 2014)) and it may provide a solution to overcome limitations of umbrella sampling and direct impinging simulations.

This paper presents a molecular simulation study aimed at revealing the mechanism of water uptake in a vapor/hydroxy-*cis*-pinonic acid/water double interfacial system at two temperatures representative of the planetary boundary layer and the top of the troposphere. Free energy profiles of water uptake are generated using steered MD simulations, and are used to describe the temperature dependence of the water uptake mechanism. Thermodynamic driving forces are identified by decomposing the free energy profiles into entropic and enthalpic contributions. Knowing the molecular scale mechanism of water uptake, the useability of a single mass accommodation coefficient to describe gas to particle partitioning is assessed. Finally, different scenarios through which LLPS affects cloud droplet activation and growth are identified and tested in the framework of the Köhler-theory.

2 Methods

2.1 Technical background

The molecular scale mechanism of water uptake is assessed via the analysis of free energy profiles. This approach allows us to follow the entire gas-to-particle partitioning process. Free energy calculations using molecular simulations are challenging as in statistical thermodynamics free energy is a function of the total partition function which cannot be calculated from finite length equilibrium molecular simulations. Molecular simulation methods to calculate free energy profiles, among them umbrella sampling and steered molecular dynamics, often rely on forcing the system to follow a pathway along an aptly chosen set of reaction coordinates, which are functions of the atomic coordinates and provide a low dimensional representation of the physical process. In umbrella sampling the reaction coordinate space is mapped in a set of consecutive equilibrium simulations, with the value of the reaction coordinates constrained at a different value in each simulation. The average force needed to constrain the value of the reaction coordinate is then integrated across all the simulations. This method reproduces the process in quasi equilibrium steps at an infinitely low velocity. Free energy profiles obtained that way thus neglect the effect of friction. In steered MD the system is pulled along the reaction coordinate space with the help of an external harmonic bias at a constant finite velocity or with a constant finite force and the work exerted by the harmonic bias is used to reproduce free energy profiles. Finite velocity pulling ensures that that the effect of friction is taken into account in the simulations. The steered MD method is illustrated in Figure 1. Sample steered MD trajectories are available as video supplement.

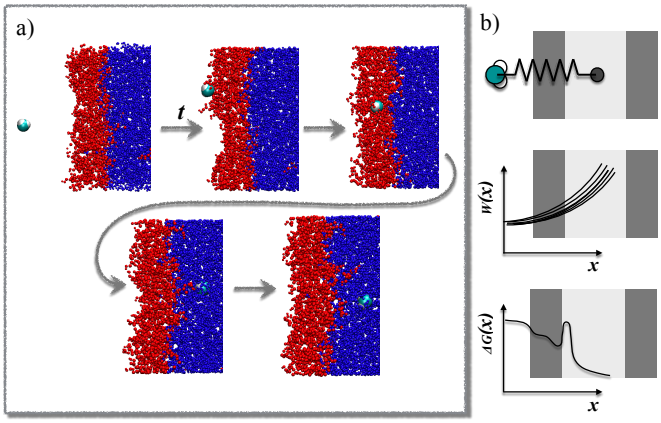

Figure 1. a) Example of the evolution of a steered MD simulation. b) Schematic summary of the free energy reconstruction protocol.

According to the second law of thermodynamics only an uppper estimate of the equilibrium free energy related to a process can be inferred from the work accompanying the transition that occurs at finite speed. In a process captured by a time dependent

reaction coordinate $s = s(t)$ the free energy change $\Delta G_{s_0}^{s_t}$ can be related to the average work ($\langle W \rangle$) by:

$$\Delta G_{s_0}^{s_t} = G_{s(0)} - G_{s(t)} \leq \langle W \rangle. \tag{1}$$

In this framework equality holds solely in case of infinitely slow transitions, performed in equilibrium steps, with no dissipation involved. In his pioneering work, Jarzynski found an analogous expression for which equality is valid regardless of the speed of the transition:

$$e^{-\beta \Delta G} = \langle e^{-\beta W} \rangle, \tag{2}$$

where $\beta = 1/k_B T$ and k_B is the Boltzmann constant and T is the temperature. Jarzinsky's discovery opened up the possibility of estimating free energy differences from non-equilibrium processes, such as AFM or single molecule experiments. Free energy profiles can be reconstructed in a similar manner using the reweighting scheme introduced by Hummer and Szabo. Every pulling experiment or simulation relies on attaching a harmonic spring to the molecular system in the direction of the reaction coordinate ($s(\mathbf{x}, t)$)), which exerts an external bias on the systems with coordinates ($\mathbf{x}$) which manifests in the Hamiltonian as $H(\mathbf{x}, t) = H_0(\mathbf{x}) + V[s(\mathbf{x}, t)]$, with $V[s(\mathbf{x}, t)]$ being the potential of the harmonic oscillator. The unbiased free energy profile along s can thus be reconstructed from the time dependent work profiles by removing the external bias caused by the harmonic potential according to Equation 3, derived in (Hummer and Szabo, 2001), which represents a weighted histogram over a sufficiently large number of trajectories:

$$e^{-\beta G(s)} = \frac{\sum_t \frac{\langle \delta[s - s(t)] e^{-\beta W_t} \rangle}{\langle e^{-\beta W_t} \rangle}}{\sum_t \frac{e^{-\beta V(s,t)}}{\langle e^{\beta W_t} \rangle}}, \tag{3}$$

where $\langle ... \rangle$ denotes averaging over parallel realizations.

2.2 Simulation details

Steered MD simulations are performed using the GROMACS 5.1.3 program package. (Abraham et al., 2015) The PLUMED 2.5 plugin (Tribello et al., 2014); is used to implement and control the collective variable and other parameters specific to steered MD simulations. The system consisting of a rectangulart slab containing 5000 water molecules enclosed between two multilayers of hydroxy cis-pinonic acid (h-CPA), containing 125 molecules each. The liquid slab is surrounded by a vapor phase from both sides (Figure 1). The average widths of the layers along the Z axis of the simulation box are ~ 6.5 nm, ~ 2.5 nm and ~ 6 nm for water, CPA and the vapor phase, respectively. The protocol to create and equilibrate such interfacial systems is described elsewhere. (Hantal et al., 2010; Darvas et al., 2011b) A single water molecule is placed in the vapor phase of the preequilibrated interfacial system and pulled towards the middle of the aqueous phase along the reaction coordinate ($s(\mathbf{x}, t)$) defined as interface-normal (Z) component of the distance connecting its center of mass to that of the aqueous phase by harmonic bias having a spring constant k=1000 kJmol^{-1}nm^{-1} at a constant pulling velocity ~ 1.5 nmns^{-1}. This condition

satisfies the stiff spring approximation (Hummer and Szabo, 2001) which makes it possible to reconstruct the free energy profiles according to the scheme of Hummer and Szabo and enables the system to closely follow the path of the reaction coordinate by becoming the dominant force in the total dynamics. A similar reaction coordinated has been used recently to study gas-to-particle partitioning by well-tempered metadynamics.(von Domaros et al., 2020)

100 parallel 6 ns-long realizations are performed at two temperatures, 200 and 300 K on the NVT ensemble. The realizations differ in the initial position of the gas phase water molecule in the X,Y plane parallel to the surface of the liquid slab, and in the random seed which is used to set initial velocity distributions. Temperature is kept constant by means of the V-rescale thermostat (Bussi et al., 2007). Water molecules are described by the TIP4P water model (Jorgensen et al., 1983) and h-CPA molecules by the OPLS potential (Jorgensen and Tirado-Rives, 1988). Alkyl groups are treated as united atoms, while other hydrogens are treated explicitly. Long range electrostatics are accounted for by the particle mesh Ewald method (Essmann et al., 1995) beyond a cutoff of 1 nm, while Lennard-Jones interactions are smoothly truncated to zero beyond the same cutoff.

3 Results and discussion

In the following sections free energy profiles are interpreted in terms of the local characteristics of the simulated systems and a detailed mechanism of water uptake is proposed. The decomposition of the free energy profiles into enthalpic and entropic contributions allows us to identify thermodynamic driving forces of interfacial mass transfer of water in LLPS SOA. The effect of the complex water uptake mechanism on particle growth and activation is then assessed by estimating interfacial transfer coefficients. Implications for atmospheric systems are highlighted via model calculations.

3.1 Thermodynamic description

3.1.1 Intrinsic density profiles

Local nanoscale fluctuations of fluid interfaces due to capillary waves create surface corrugations (Chowdhary and Ladanyi, 2008; Jorge et al., 2010) characterized by amplitudes ranging between 0.3 and 1 nm depending on the chemical composition of the surface(Hantal et al., 2010; Darvas et al., 2011a), which do not average out during typical timescales associated with mass transfer from the vapor to the particle phase in the atmosphere. Intrinsic surface analysis (Appendix A) of molecular simulation trajectories is necessary to resolve the effect of capillary waves on density(Jorge et al., 2010) and free energy profiles(Darvas et al., 2013; Braga et al., 2016). In this work intrinsic analysis is limited to the selection of surface atoms and the calculation of density profiles anchored to the fluctuating surface by the ITIM algorithm(Sega et al., 2018), which allows to establish qualitative connections between the free energy profiles and the local properties of the interfacial system.

Shaded blue and yellow areas in 2 a) and b) show the intrinsic mass density profiles of the aqueous and the organic phase. Organic density profiles reveal that the thickness of the organic phase is ~ 1.8 and ~ 2.1 nm at 200 and 300 K respectively, measured at 5% of the average height of the profile. It is sufficient to accommodate a disordered multilayer, but is too low to allow the formation of a bulk phase. The lack of a bulk phase is evidenced by the two neighboring Gaussian peaks –

characteristic of interfaces – in the density profile of the organic phase with no plateau at the bulk phase density (1200 $kgm^{-}3$)in between. An $\sim 85\%$ drop in total local total density (sum of water an organic density) compared to that of bulk aqueous phase can be observed at the Gibbs dividing surface of the two condensed phases at both temperatures, albeit the affected region is wider at 300 K. The aqueous phase has two consecutive peaks characteristic of the first two molecular layers, followed by a bulk phase plateau. The interface and subsurface structure is similar but more pronounced at 200 K as result of reduced thermal motion which preserves layered structure at low temperatures. The interfacial region is characterized by an overlap between the organic and the water density profiles, which – alike the small peak of organics in the bulk aqueous phase – is due to partial miscibility of the two phases. The width of this mixed region is 1.5 nm at 300 K and 1.2 nm at 200 K disregarding the small peak of organics in the bulk aqueous phase.

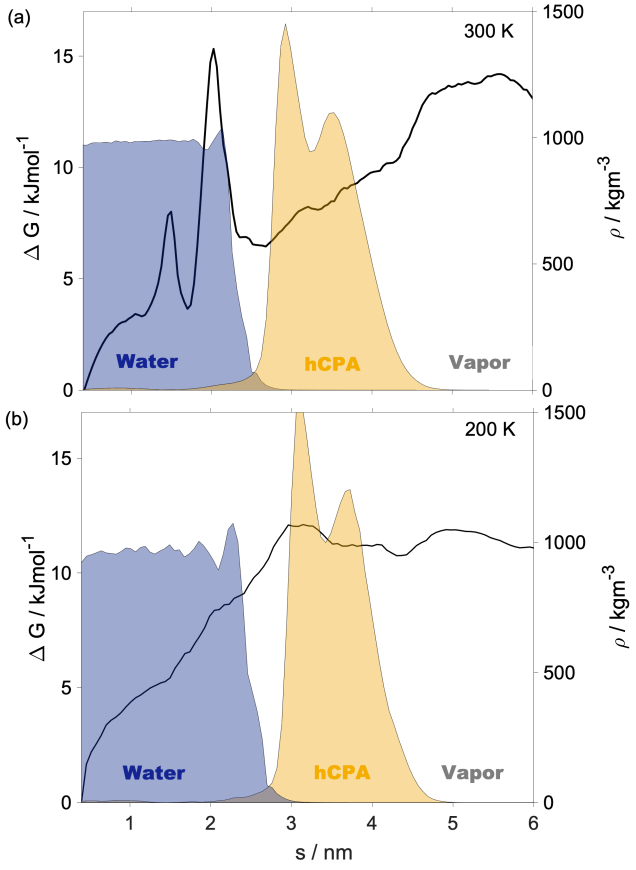

Figure 2. a) Free energy and density profiles at T=300 K; b) the same profiles at T=200 K

3.1.2 Free energy profiles

Free energy profiles with the reference state assigned to the bulk aqueous phase are shown as black solid lines in Figure 2 a) and b). Profiles are significantly different at the two temperatures which suggests that mechanism of gas-to-particle partitioning is LLPS particles is temperature dependent, however, they show two main common characteristics: i) the negative free energy difference (~ -14 kJmol^{-1} at 300 K and ~ -11 kJmol^{-1} at 200 K) between the bulk aqueous and the vapor phase, which underlines that overall water uptake from the vapor phase is thermodynamically favored; and ii) the lack of a free energy barrier at the vapor/organic interface, which is the main difference between free energy profiles of transfer through hydrophobic media, for which large maxima have been observed leading to reduced surface accommodation coefficients. (Ergin and Takahama, 2016) The free energy profile at 300 K begins with a plateau characteristic of the vapor phase, followed by a steep decrease (~ 5 kJmol^{-1}) at the vapor/organic interface. A monotonic decrease in the free energy profile characterizes the transfer of the water molecule in the organic phase. The lack of a plateau is related to the fact that the organic layer is not thick enough to accommodate a bulk phase, which results in a position dependent anisotropy caused by the proximity of both interfaces in combination with the partial dissolution of the water in the organic phase, evidenced by non-zero water density up to s≈ 3.5 nm. The effect of the presence of dissolved water molecules manifests in an increased slope of the profile near the water/organic interface. The free energy profile has a local minimum at the organic/water interface, and a global maximum (~ 14 kJmol^{-1}) corresponding to the first molecular layer of water, seen as a peak in the intrinsic density profile, followed by a second peak and smoothly decreasing region.The free energy profile at 200 K is considerably smoother than the room temperature one. The free energy drop accompanying the attachment of the pulled water molecules to the organic phase is reduced to ~ 1 kJmol^{-1}, which is smaller than the energy of thermal motion ($3/2k_BT$) at the given temperature, and is thus statistically insignificant, similarly to the small minimum at the interface. Similar considerations are valid for the small maximum found at the organic side of the organic/water interface. The minimum and the peak at the organic/water interface characteristic of the room temperature profile cannot be observed at low temperature. Comparison of two free energy profiles indicate that the detailed mechanism of water uptake – up to the aqueous core of the particle – is temperature dependent. While vapor-to-organic transfer is a favorable and barrierless transition at both temperatures, the transport between the organic shell and the core is thermodynamically hindered by the presence of the free energy barrier at 300 K, which diminishes at low temperature. Large differences between the free energy profiles obtained at the two temperatures suggest that the thermodynamic driving forces which govern the shape of the profiles are strongly temperature dependent. One possible explanation is that main driving forces are of entropic natrure, and their strength is explicitly scaled by the temperature through the $-T\Delta S$ term of the free energy.

3.1.3 Enthalpy and entropy profiles

To understand the thermodynamic driving forces which govern the water uptake mechanism, free energy profiles are decomposed into entropic and enthalpic contributions, which are shown in Figure 3. The sum of interaction energies of the pulled water with the surrounding molecules is used as a surrogate for the enthalpy, the calculation is described in details in Appendix B. Alike for free energy profiles, the bulk aqueous phase is chosen as the reference state. The total entropy profile is obtained by

subtracting the enthalpy profile from the free energy profile, and some distinct contributions to the total entropy are calculated. We note that neither the additivity nor the completeness of entropy terms is ensured in this analysis. The entropy contributions that are analysed in details were selected to explain the features of the free energy profiles.

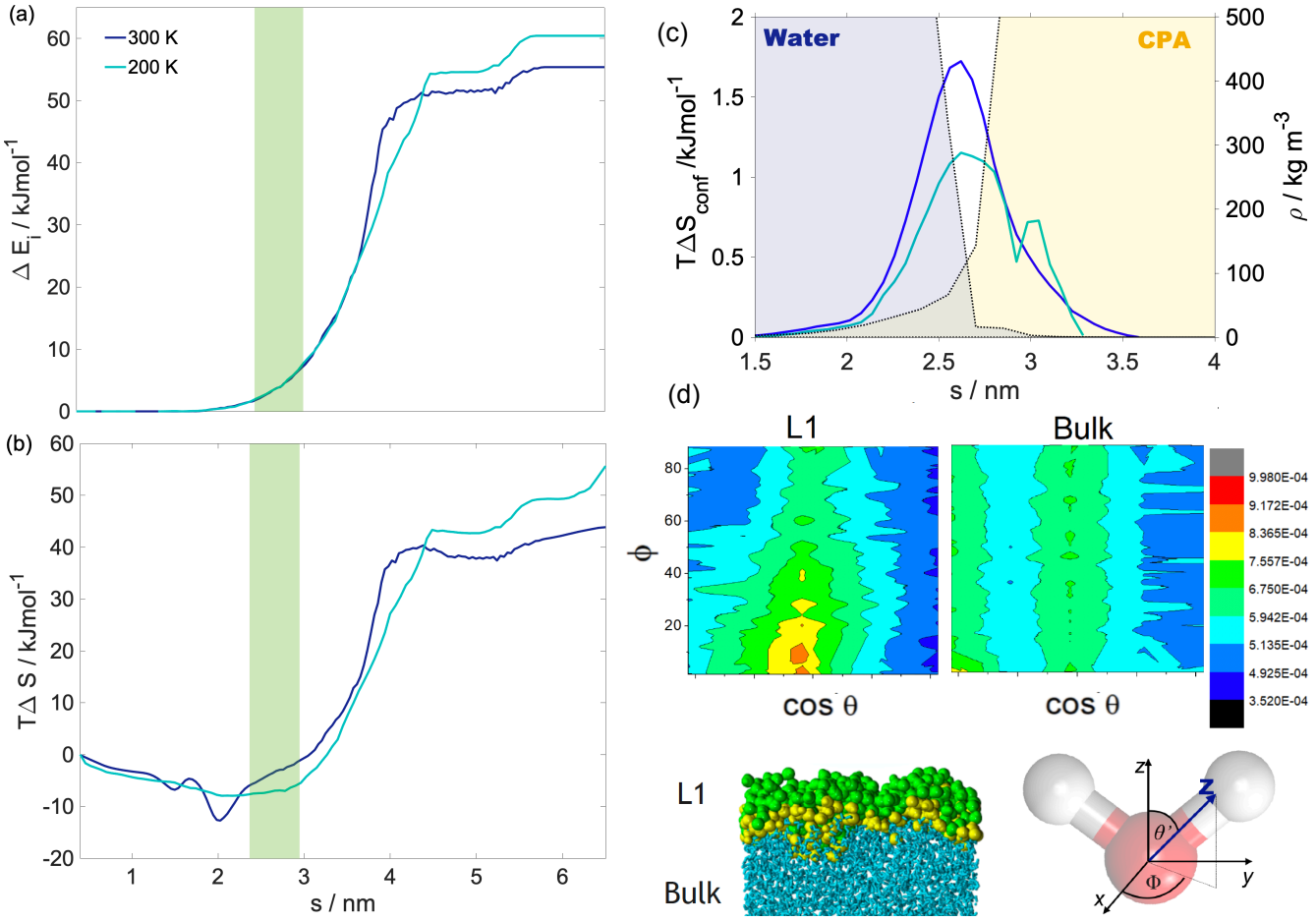

Figure 3. a) Enthalpy, b) entropy profiles as a function of the reaction coordinate used in the steered MD simulations, the green shaded area denotes the interfacial region between the organic and aqueous phase c) The conformational entropy in the interfacial region overlapped with intrinsic density profiles of the aqueous (blue shaded) and the organic (yellow shaded) phase d) Top panel: Orientational maps of the water molecules in the first molecular layer (L1) of the aqueous phase and in a randomly selected layer in the bulk phase. Bottom panel left: An equilibrium snapshot from a simulation showing the first two molecular layers (green and yellow balls) and the bulk phase (cyan sticks) as determined by the ITIM algorithm. Bottom panel right: the definition of the orientational vectors of the water molecule.

240 Enthalpy profiles in Figure 3 a) show that water uptake is energetically favorable, the enthalpy difference between the pulled water molecule being in the vapor phase and in the aqueous phase is ~ -55 kJmol^{-1} at 300 K and ~ -60 kJmol^{-1} at 200 K. This corresponds approximately to the formation of 3-4 hydrogen bonds by the pulled molecule, which is also supported

by the hydrogen bond profile calculated for a randomly selected realisation (A). The energy of a water-water hydrogen bond is approximately 20 kJmol^{-1} based on quantum chemical calculations, while that between is h-CPA and water is unknown. Enthalpy profiles are smooth and show a similar overall behavior at the two temperatures. A small drop in the enthalpy whose magnitude is ~ 3 kJmol^{-1} and ~ 5 kJmol^{-1} at the 200 and 300 K respectively indicates the formation of contact with the organic phase. It is however not sufficiently low compared to the enthalpy observed in the subsequent bulk organic phase to energetically stabilise a surface adsorbed state. Both enthalpy profiles have a plateau spanning the outer half of the organic phase, where water molecules from the bulk aqueous phase do not penetrate. This is followed by a smoothly decreasing part which corresponds to the pulled molecule forming an increasing number of hydrogen bonds with both h-CPA and the water molecules dissolved in the organic phase. Near the organic-water interface and in the aqueous phase the enthalpy profiles are close to indentical. The similarities of the enthalpy profiles at the two temperatures suggests that specific features of the free energy profile are of entropic origin.

Total entropy profiles bear all the features that appear in the free energy profiles and their shape is different at two temperatures. In the following these profiles are further decomposed into specific entropy terms, such as configurational, conformational and orientational entropy. Configurational entropy profiles calculated using Schlitter's formula(Baron et al., 2006) as explained in Appendix B are close to constant throughout the condensed phase, $-T\Delta S_{config} = 25$ kJmol^{-1} at 300 K and 14 kJmol^{-1} at 200 K. They are thus not responsible for any of the features in the free energy profiles. Interfacial entropy ($T\Delta S_{IF}$) at the vapor/organic interface is approximately 5 kJmol^{-1} at 300 K and is negligibly small at 200 K (Appendix B). Despite of the positive value of interfacial entropy the overall entropy difference between the vapor and the organic phase is a small negative value, which - together with the moderate change in enthalpy at the interface - is responsible for the lack of surface adsorbed state. A possible explanation for the overall negative entropy is related to the ordering of the organic molecules at the surface which reduces orientational degrees of freedom in a similar manner than that described later for the water/organic interface. Conformational entropy profiles, calculated from the mole fraction profiles of the water and the organic molecules (Appendix B) are shown in Figure 3) c). They have pronounced peaks near the organic organic/water interface and their values are close to zero elsewhere. These peaks highlight the effect on non-ideal local mixing between of the two phases in this region. A slightly larger value of the conformational entropy at 300 K, which is an explicit effect of the temperature, partly explains the higher entropy in this region. The higher conformational entropy is accompanied by an $\sim 85\%$ decrease in the total density in this region. Lower density ensures the reduction of steric hindrance for any conformations without loosing hydrogen bonds, which explains the minimum in the free energy profile observed at the water/organic interface at 300 K. High conformational degrees of freedom manifest in subsequent detaching/attaching of the pulled molecule between the organic and aqueous phase in varying orientations, which can be observed only in the 300 K simulations (video supplement available). The conformational entropy profile shows a significantly ($\sim 40\%$) smaller peak in the interfacial region at 200 K. Additionally, the low density region is narrower due to the pronounced shoulder in the water density profile (Figure 2), thus steric hindrance is not as effectively reduced as at 300 K. The joint decrease of the strength of the two entropic contributions leads to the disappearance of the free energy minimum at the organic/water interface at 200 K. Increased orientational order of molecules constituting the first few layers of molecular liquids leads to a reduced orientational entropy, which is responsible for the free energy peak coincid-

ing with the first two molecular layers of water in the 300 K simulations. To illustrate the differences between the orientational preferences of interfacial and bulk water molecules we calculate the joint distribution of the two angles defined in the bottom right panel of Figure 3 d) in the first molecular layer and in a randomly selected molecular layer from the bulk. Details of the calculation are summarized in (B).The two dimensional joint distribution of these two angles (Figure 3 d), top panel) is able to define the orientation of a rigid body having a C_{2v} point group symmetry with respect to an external axis. The peak shows that in the first layer water molecules tend to lie parallel to the surface, whereas bulk phase distribution bears no evidence of preferred orientations. Increased orientational order results in a decrease in orientational entropy, which corresponds to the maximum in the free energy profile. We note that the second layer of water has similar orientational preferences (Appendix B, which explains the subsequent smaller peak. Similar orientational preferences are found for 200 K (B). The observed temperature dependence results from the explicit scaling of the importance of entropy with temperature. Orientational entropies are estimated along one dimension of the orientational maps (Appendix **??**), and show strong temperature dependence. We acknowledge that the one dimensional representation is incomplete and thus gives only a qualitative insight, the extension of the orientational entropy formula to multiple dimensions is part of an ongoing project.

3.1.4 Generalization of the driving forces

The most prominent characteristics of the free energy profile are the lack of a minimum at the vapor/organic interface, the minimum at the organic/water interface and the maximum corresponding to the first layer of the aqueous phase. Previous molecular simulations studies show that driving forces which lead to the appearance of these features are generally present in interfacial systems involving molecular liquids or solids. The value of the free energy at the vapor/organic interface is moderated by the increased order of organic molecules which has been seen for pure organics(Darvas et al., 2010a) as well as for concentrated(Darvas et al., 2010b) and dilute aqueous organic solutions(Pártay et al., 2008; Pojják et al., 2010) Both density drop in the interfacial region and local mixing which invoke the free energy minimum at the organic/water interface at 300 K are characteristic of any liquid/liquid interface(Hantal et al., 2010; Jorge et al., 2010; Darvas et al., 2011b, 2013). The extent of local mixing is trivially determined by the hydrophylicity of the organic compound. Orientational preferences of water molecules near liquid/liquid, liquid/vapor or liquid/solid interfaces, which account for the maximum of the free energy profiles are also generally present in interfacial systems. Interfacial molecules adapt preferred orientations owing to topological anisotropy of intermolecular interactions, in contrast to the bulk where isotropic energetic environment ensures random orientations. Preferential orientations of interfacial water molecules have been observed in molecular simulations several times at various liquid/liquid interfaces such as carbon tetrachloride(Hantal et al., 2010; Kertész et al., 2014) or dichloroethane(Hantal et al., 2010), as well for liquid/vapor interfaces of pure water(Bartok-Partay et al., 2008) and aqueous mixtures and organic compounds(**??**Darvas et al., 2011b). Orientational preferences proved to be enhanced next to a solid counter phase.(Kertész et al., 2014). Furthermore the strong temperature dependence follows directly from the entropic nature of these driving forces and the definition of the free energy, thus temperature dependence thus besides the presence of the features their temperature dependence is also expected to be generally valid. This ensures that our findings are not system specific, and represent a typ-

ical behavior for sparingly soluble organic compounds present in the atmosphere. A systematic quantitative study of relevant interfaces is subject of ongoing work.

3.2 Implications for water uptake and particle growth kinetics

3.3 Interfacial transfer coefficients

Interfacial transfer coefficients are estimated from the activation free energies characteristic of the vapor-to-organic (α_{vo}), organic-to-water (k_{ow}) and vapor-to-water (k_{vw}) transfer using the transition state theory as:

$$k_{ij} = exp\left[\frac{-\Delta_{ij}^{\#}G}{RT}\right], \tag{4}$$

where i and j indicate the phases forming the interface in question.The corresponding activation free energies are illustrated using the 300 K free energy profile in Figure 4 a). We note that due to the lack of a well-defined bulk phase plateau in the organic phase we choose an average value characteristic of the middle of the organic phase as a reference value. This choice is arbitrary and a different definition of the organic phase reference may result in slight shifts in the obtained transfer coefficient, albeit without altering trends and conclusions. Vapor-to-organic (surface) a transfer coefficient (k_{vo}) are near unity at both temperatures, whereas organic-to-water transport is characterized by $k_{ow} = 0.05$ at 300 K, and $k_{ow} = 1$ at 200 K. To complete the analysis we estimate a hypothetical transfer coefficient of the uptake of water from the vapor phase by the aqueous core disregarding the organic phase, k_{vw} which is equal to 0.38 at 300 K and unity at 200 K.

Vapor-to-organic transfer coefficients are the most closely related to the commonly used definition of the mass accommodation coefficient, which considers either adsorption at the surface or absorption in the first few molecular layers of the particle phase as the final state of gas-to-particle partitioning. Due to the lack of maxima or minima at the vapor/oragnic interface, in our systems surface adsorbed states of the water are thermodynamically indistinguishable from those with the water absorbed by the subsurface region. Near unity vapor-to-organic transfer coefficients agree well with the globally representative values of surface accommodation coefficients(Raatikainen et al., 2013) and with recent experimental findings which evidence large mass accommodation coefficients(Liu et al., 2019) and non-hindered gas-to-particle partitioning of water and organics in phase separated particles. (Gorkowski et al., 2017)

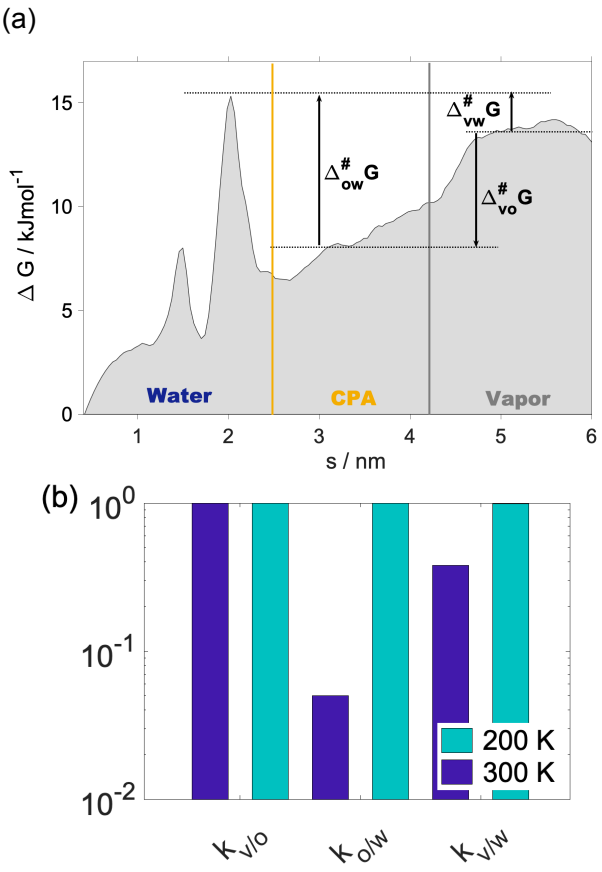

Figure 4. a) Definition of activation free energies at the different interfaces at T=300 K. b) Transfer coefficients at the different interfaces dark blue 300 K, light blue 200 K

Closely packed continuous hydrophobic organic films can result in mass accommodation coefficients as low as 0.001, and values of α are found to be strongly correlated tothe integrated carbon number density(Ergin and Takahama, 2016) of the organic layer, which is estimated as the integral of the density profile along the outer half of the organic layer divided by its width. The integrated carbon number density for our systems is 14 nm^{-3} which for a completely hydrophobic film comprised solely of aliphatic CH moieties would correspond to in $\alpha \sim 0.01$(Ergin and Takahama, 2016) instead of the observed near unity values. In the presence specific interactions, hydrogen bonds and dipole-dipole interactions, of hydrophilic functional groups such a simple descriptor is insufficient to the predict reliable mass-accommodation coefficients. Mass accommodation coefficients on the less hydrophobic disordered multilayer of h-CPA are expected to be larger due to the availability of hydrogen bonds already near the organic surface which make the surface accommodation of water thermodynamically favorable, while orientational entropy will prevent the formation of long-lived surface adsorbed states.

The organic-to-water (k_{ow}) and vapor-to-water transfer coefficients (k_{vw}) are reduced compared mass accommodation coefficients (k_{vo}) at room temperature owing to the free energy barrier corresponding to the first molecular layer of water, which is due to lower orientational entropy is higher density compared to the bulk phases As opposed to mass accommodation coefficients which show no temperature dependence, k_{ow} and k_{vw} follows a similar trend with temperature as that observed for water uptake on a hexadecanol monolayer(Davies et al., 2013), and on pure water (Davidovits et al., 2004). Organic-to-water transfer coefficients describe the lower bound of the probability of a gas phase water molecule being absorbed by the aqueous core of the phase separated particle. Vapor-to-water transfer coefficient represent an upper bound of the same probability. Thus k_{ow} and k_{vw} define the range of core uptake coefficients. The fact that core uptake coefficients differ significantly from mass accommodation coefficients highlights the possibility that the traditional representation of water uptake by a single value of α has to be completed by a temperature dependent core uptake term to describe water uptake by phase separated aerosol in more realistic manner.

3.3.1 The effect of mass accommodation coefficients

It is established that reduced mass accommodation coefficients result increased CCN number concentrations. The explanation for this effect is that droplet number concentrations in ambient clouds depend on the maximum supersaturation, S_{max}, which is largely determined by the condensation rate of water vapor on the growing droplets. Reduced α values correspond to low condensation rates which result in increased S_{max} and consequently, larger droplet concentrations and increased CCN activity. Models simulations predict a mild 1.2-fold increase in CCN number concetrations for $\alpha = 0.1$, a 1.5-1.8-fold increase for $\alpha = 0.01$ and 2-2.5 fold increasee for $\alpha = 0.001$. (Raatikainen et al., 2013). In this framework, near unity mass accommodation coefficients obtained from our simulations at both temperatures are not expected to alter droplet number concentrations by causing kinetic delays. This finding is in line with the observation that global datasets can usually be described by $0.1 < \alpha < 1$, implying uninhibited water uptake.

3.3.2 The effect of core uptake coefficients

Hindered mass transfer of water between the organic shell and aqueous core together with uninhibited mass accommodation of water in LLPS aerosol results in different condensational growth rates of the core and shell. In other words, a dynamic retention of water by the organic shell can be observed. We use the k_{vo}/k_{ow} ratio to estimate the extent of dynamic retention of water by the organic phase, the physical meaning of this ratio is the number of vapor-to-organic transfers occurring for one organic-to-water transfer. The value is approximately one at 200 K while a 20-fold retention is observed at 300 K. The growth rate of the organic shell is thus substantially larger at 300 K than that of the core, which in agreement with results of multilayer kinetic model (KM-GAP) calculations which also evidence faster condensational growth of the particle shell than of core.(Shiraiwa et al., 2013) This suggests that the aqueous core contains less water and the organic shell is more dilute at any time during growth of the particle than what is predicted assuming that mass transfer kinetics can be described by a single value of α.

Retention of water in the organic shell due to reduced core uptake coefficient may affect equilibrium properties (vapor pressure and surface tension) which determine cloud droplet growth and activation. Increased water content of the organic shell can result increased vapor pressure and surface tension, which both affect cloud droplet growth and activation via the Köhler theory. This hypothesis is valid if the vapor phase is in dynamic equilibrium with the organic shell containing an increased amount of water and this equilibrium is unaffected by the presence of the aqueous core. For this condition to hold gas-to-particle partitioning timescale of water (tau_s) should be significantly shorter than timescale of transfer from the shell to the core (tau_c). Timescales are calculated assuming that both gas-to-particle and shell-to-core partitioning can be described as(Saleh et al., 2013):

$$\tau = \frac{1}{2\pi DFd}, \tag{5}$$

where $F = (1+Kn)/(1+0.3773Kn+1.33Kn(1+Kn)/\alpha)$ is the Fuchs-Sutugin correction factor, with Kn being the Knudsen number and α the transfer coefficient of the given process. For gas-to-particle partitioning $Kn = 10^{-2}, 10^{-1}, 10^{0}$, $\alpha = 1$, the gas phase diffusion coefficient of water is estimated at 0.26 cm^2s^{-1} and 0.128 cm^2s^{-1} at 300 and 200 K (**?**), while d is the diameter of the particle. For core-to-shell partitioning Kn is approximated as the ratio of the diameter of the h-CPA molecules and the width of the organic layer, $\alpha = k_{ow}$ in one set of calculations and $\alpha = k_{vw}$ in another set, d is the core diameter, and the diffusion coefficient(D) is varied between $10^{-3}$and 10^{-8} cm^2s^{-1}. The $\tau_c/\tau_s > 10^{-3}$ in every case (Figure 5), thus the hypothesis of equilibrium holds for our system at both temperatures.

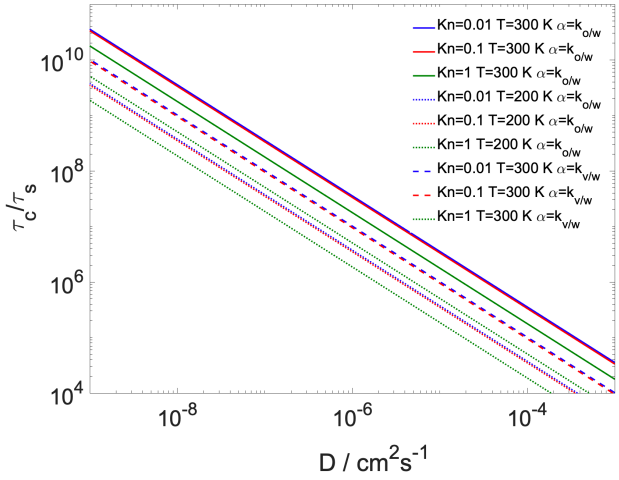

Figure 5. The ratio of characteristic timescales of shell-to-core and gas-to-particle partitioning as function of bulk phase diffusivity of the water in the organic shell at varying gas phase Knudsen numbers and temperature. At 300 K model calculations are presented using both the lower and the upper of the core uptake coefficient.

Finally,inhibited water transport between the shell and the core of the particle may result in the swelling and – depending on the solubility of the organics – the dissolution of the organic shell.

3.3.3 The effect of bulk diffusion and non-uniform concentration distribution

A non-negligible free energy difference exists between the vapor/organic and the organic/water interface which potentially alters the above described uniform increase of the water concentration in the shell and its consequences for droplet growth and activation. A more detailed understanding of the effect of accumulated water in the organic shell on particle growth can be obtained by converting the free energy profile using the expression $\Delta G(s) = -k_B T ln c_{rel}(s)$ into a probabilistic density profile $c_{rel}(s)$, which can be interpreted as an equilibrium concentration profile (Figure 6) of the condensing water in the organic phase at arbitrary values of the vapor pressure. This conversion yields equilibrium concentration profiles under the assumption of instantaneous diffusion and bears no information about the surrounding relative humidity (RH). The effect of non-instantaneous bulk phase diffusion and RH accounted for by a correction factor, f:

$$\mathrm{c}_{rel}(s) = exp\left[\frac{-\Delta G(s)}{k_B T}\right] f(D_p, C_v)$$

$$f(D_p, C_v) = \frac{1}{1 + \frac{\alpha \omega C_v}{4 D_p \rho_p s}},$$

where $f(D_p, C_v)$ is a correction factor with C_v and D_p being the vapor phase concentration of water and the bulk phase diffusion coefficient of water in the organic phase. ω is the mean thermal velocity of water in the vapor phase, α is the mass accommodation coefficient and ρ_p is the density of the organic phase (1.2 gcm^{-3} in our calculation). The correction factor was adapted from a recent work (Shiraiwa and Pöschl, 2020) which derived an expression to account for the effect of diffusivity on gas-to-particle partitioning by introducing a penetration depth dependent definition of the mass accommodation coefficients of organic molecules absorbed by aerosol particles used in particle growth kinetic models.(**?**Shiraiwa et al., 2012). Our model calculations are performed at five RH values in the range of 50-98%; using 13 different diffusion coefficients between 10^{-15} and 10^{-3} cm^{2}s^{-1}, characteristic of liquid and semisolid particles. $c_{rel}(s)$ is normalized to the 0-1 range, with 0 and 1 corresponding to the minimum and maximum of the $c_{rel}(s)$ function within the organic phase at 300 K.

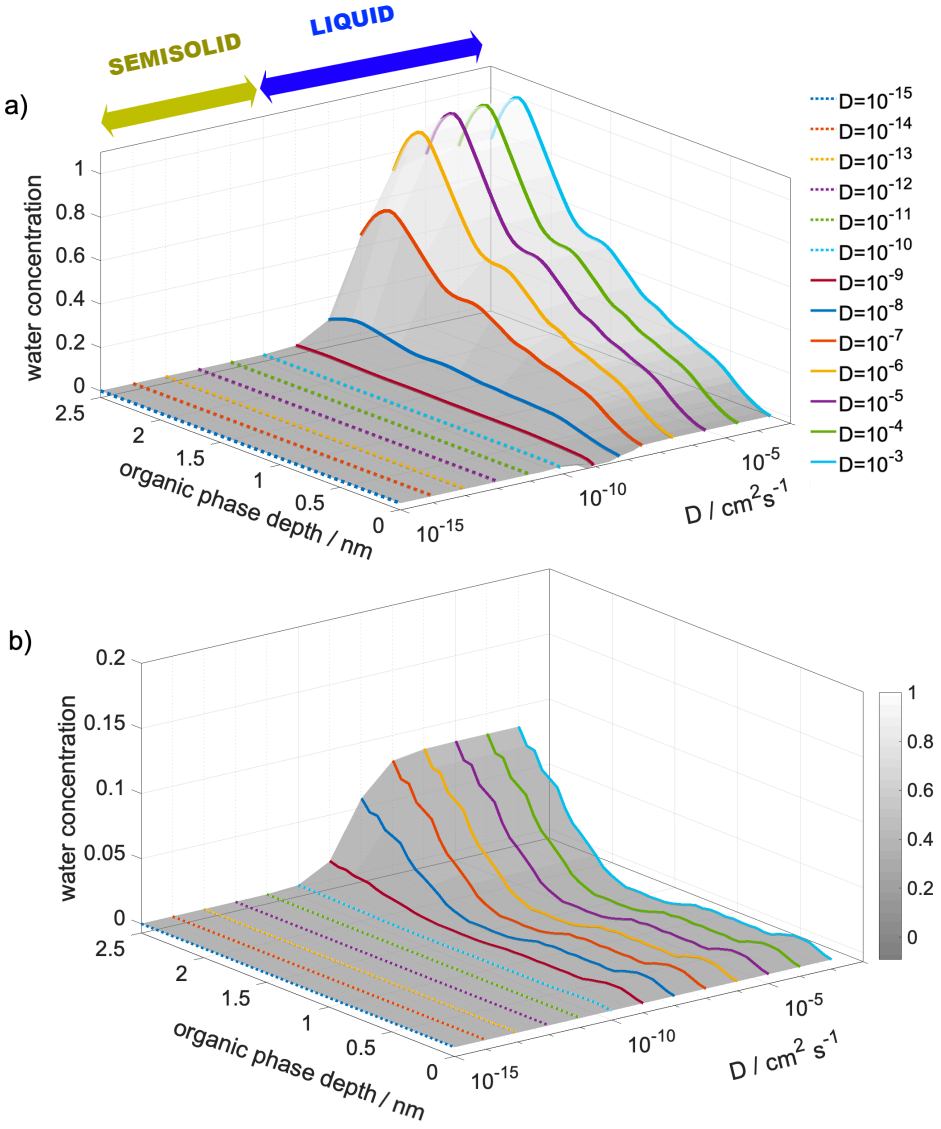

Figure 6. Modeled, diffusivity-corrected concentration gradient of water in the organic phase at a) 300 K and b) 200 K at 98% RH and at varying diffusion coefficients. Organic phase depth describes the distance from the vapor/organic interface, zero corresponds the Gibbs dividing surface between the vapor and particle phase

Figure 6 equilibrium diffusion corrected concentration profiles at RH=95%. Condensing water molecules show a strong preference to be accommodated near the organic/water interface, while the vicinity of the vapor/organic interface is depleted in water at 300 K (Figure 6) a)) for bulk phase diffusion coefficient values characteristic of the liquid phase ($10^{-3} < D_p < 10^{-9}$ cm^{2}s^{-1}). A much less pronounced concentration gradient, about an order of magnitude smaller than that found at room temperature, can be observed at 200 K if liquid phase diffusivities are assumed. The effect of diffusion is negligible in $10^{-3} < D_p < 10^{-6}$ cm^{2}s^{-1} diffusivity range. The steepness of the concentration gradient is reduced by 40 and 85% for $D_p = 10^{-7}$ and $D_p = 10^{-8}$ cm^{2}s^{-1} at 300 K, and by 30 and 82% for $D_p = 10^{-8}$ and $D_p = 10^{-9}$ cm^{2}s^{-1} at 200 K. Slow diffusion in highly viscous liquid and semisolid states ($D_p < 10^{-10}$ cm^{2}s^{-1}) cancels the effect of thermodynamic preferences, and result in uniform concentration profiles at both temperatures. Concentration profiles are not sensitive to varying RH, thus only one characteristic example is shown in Figure 6. Water's diffusion coefficient in h-CPA is estimated from separate unpublished MD simulations to be $10^{-5} - 10^{-6}$ cm^{2}s^{-1} at 300 K depending on concentration, and $10^{-7} - 10^{-8}$ cm^{2}s^{-1} at the lower temperature, similar values have been also reported based on experiments (Lienhard et al., 2015). This means that room temperature concentration profiles are virtually unaffected by bulk phase diffusion, while at 200 K the originally small concentration gradient is further reduced by slow diffusion, which makes bulk phase diffusion the governing process for water uptake at low temperatures.

The concentration gradient at 300 K in liquid particles can considerably alter the effect of the accumolation of water in the shell. Alike main driving forces of the water uptake process, the formation of the concentration gradient can be expected in generic LLPS particles regardless of their actual chemical composition. The shape of the concentration profiles may change for a thicker organic layer having a bulk phase corresponding to a constant plateau in the free energy profile, which converts into a constant concentration region in the middle of the organic phase. Nevertheless, the maximum of the concentration profile coincides with the minimum of the free energy profile at the organic/water interface interface, which is determined prevalently by local entropy increase due to the lower density and increased conformational degrees of freedom, which is universal at boundaries between condensed phases. Similar considerations are valid for the minimum of the concentration profile, which is observed at the vapor/organic interface, whose value mainly depends on an interplay between intermolecular interactions, orientational order of the vapor/organic interface and interfacial entropy, which are largely insensitive to the thickness of the organic phase. The significant enrichment of the water/organic interfacial region in water may lead to a local dissolution of the organic phase. However, even when dissolution of the organic phase occurs, the strong preference of water molecules to be accommodated in the inner part of the organic shell results in depleted water concentrations at the surface, which ensures the presence of a pure organic film at the surface, and hence maintains low surface tensions despite of the elevated water concentration in the organic shell even when relative humidity approaches 100%. This is consistent with recent experiments and model calculations which conclude that LLPS persists up to very high relative humidities. (Liu et al., 2018)

3.4 Köhler curves

Based on the results of simulations and model calculation three distinct scenarios through which LLPS may affect condensational growth of particles can be identified: i) In the first scenario the LLPS is present but the core and shell growth rates

are equal as a consequence of equal mass accommodation and core uptake coefficients, the surface tension is characteristic of the saturated mixture of water and cis-pinonic acid ($\gamma = 60$ mNm^{-1})(Hyvärinen et al., 2006).This corresponds to the behavior observed at 200 K. ii) LLPS is present and only shell growth occurs while the core of the particle is intact, ($\gamma = 60$ mNm^{-1}). This corresponds to the 300 K behavior neglecting the effect of both the possible dissolution of the organic shell and the formation of a concentration gradient within the organic phase. iii) LLPS is present, solely the shell growth occurs and the surface tension is characteristic of that of the pure cis-pinonic acid ($\gamma = 30$ mNm^{-1}).(Hyvärinen et al., 2006). This represents the combined effect of hindered core uptake and concentration gradient. In order to quantify the effect of the above described scenarios, Köhler curves are calculated for particles having a 50 nm dry diameter consisting of 90% organic compounds and 10% salt and 100% organic with no salt. The obtained Köhler curves are compared with that of a well-mixed particle having the same composition.

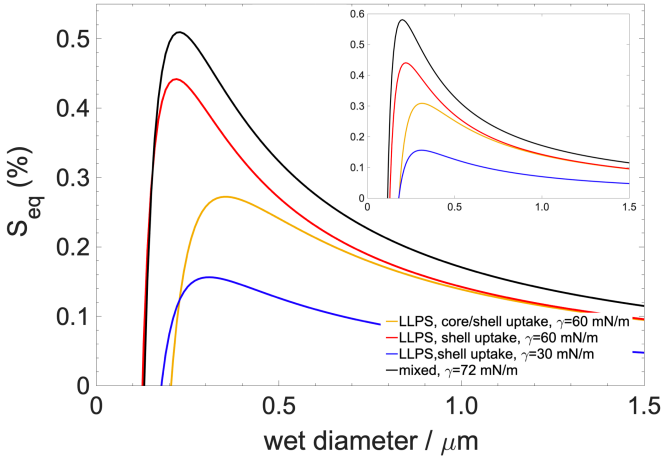

Figure 7. Köhler curves for 50 nm dry diameter particle containing 90% organic with 10% salt. The inset shows Köhler curves for a particle which contains organics only.

Figure 7 shows the Köhler curves estimated for the four different scenarios, for the two type of particles. LLPS always tends to lower critical supersaturation (S_c) and increase the critical diameter (d_c) compared to what is observed for the well mixed case. The observed lowering of the $S_c \sim 0.05$ % is the least pronounced if LLPS is preserved but only shell growth is observed, that is the scenario which describes the effect of hindered core uptake without concentration gradient. A moderate lowering of $S_c \sim 0.25\%$ is found for the low temperature scenario of LLPS with uniform core and shell growth. Whereas the effect on S_c is the strongest if the concentration gradient is taken into account, in this case the critical supersaturation is reduced by $\sim 0.35\%$.

4 Conclusions

Steered MD simulations of water uptake by a model LLPS aerosol particle consisting of a hydroxy-*cis*-pinonic acid surface layer and a pure aqueous core at two temperatures corresponding to the boundary layer (300 K) and to the top of the tropo-

sphere (200 K) were presented. Free energy profiles were calculated using Jarzynski's equality with the reweighting scheme of Hummer and Szabo. The advantage of the method over traditional approaches is that it takes friction implicitly into account without the necessity to introduce correction kernels, thus it provides a valuable alternative to MD techniques traditionally used to study gas-to-particle partitioning.

Free energy profiles and their entropic and enthalpic contributions were interpreted – for the first time in the literature – in terms of intrinsic density profiles and surface analysis which allow for an accurate description of capillary wave corrugations of liquid surfaces whose magnitude is non-negligible compared to typical sizes of aerosol particles. The overall water uptake process was found to be enthalpically driven at both temperatures, but the features of free energy profile which determine details of the uptake mechanism are of mainly entropic nature.

Free energy profiles revealed the lack of surface adsorbed states by showing the no significant minima at the vapor/organic interface; showed that vapor-to-organic transfer of the water molecule is a barrierless transition, while organic-to-water transfer is hindered at room temperature by the presence of a large peak in the free energy profile corresponding to the first molecular layer of the aqueous phase which is characterized by increased order and density, and thus lower orientational entropy. A smooth free energy profile is observed at 200 K. The substantial differences between the free energy profiles at the two temperatures suggest that the mechanism of water uptake by LLPS SOA is strongly temperature dependent, which is rooted in the entropic driving forces which form the fine structure of the free energy profile. Free energy profiles were converted into transfer coefficients corresponding to the different interfaces between the vapor and particle phase and within the particle using the transition state theory. Mass accommodation coefficients were approximated by the vapor-to-organic transfer coefficient, and turned out be near unity at both temperatures. Coefficients of water uptake by the aquoeous core were characterized by transfer coefficients ranging between 0.05 to 0.38 at room temperature, the lower bound being the organic-to-water and the upper bound the vapor-to-water transfer coefficient. All transfer coefficients were found to be unity at 200 K. The possibility that mass accommodation coefficients alter CCN number concentration for LLPS particles having relatively hydrophilic organic shells can be excluded regardless of the temperature, while the impact of low core uptake coefficients at room temperature via a strong dynamic retention of water combined with an equilibrium concentration gradient within the organic shell was analysed. The retention of water by the organic phase was shown to result in significantly more concentrated core and more dilute shell during particle growth than expected assuming unhindered core uptake. Since equilibrium between the shell and the vapor phase can be assumed due to large differences in the timescales of gas-to-particle and shell-to-core partitioning, the increased water content of the shell may lead to increased vapor pressure and surface tension compared that obtained by assuming non hindered shell-to-core transfer, and eventually to the complete dissolution of the core. Local values of thermodynamic functions, enthalpy, interfacial and orientational entropy at the vapor/organic and conformational entropy at the organic/water interface determined a probabilistic concentration profile of the condensing water in the organic phase of liquid particles, whose magnitude was found to negligible at 200 K but significant at 300 K. In semisolid particle slow diffusion cancelled the effect of thermodynamic preferences, but the gradient was at most moderately affected by diffusion in liquid particles. This concentration gradient, ensured the persistance of a pure or nearly pure organic film at the gas/particle interface, despite of the accummulation of water in the organic phase even at high RH%s, and thus that of low surface tensions. Köhler curves showed

that low surface tension due to the concentration gradient and LLPS significantly reduce equilibrium supersaturations, which is in agreement with experimentally observed increased CCN activity of LLPS particles.

The strong temperature dependence of the water uptake mechanism together with the importance of the core uptake coefficient and of the non-uniform distribution of water within the organic shell suggest that a detailed description of water uptake including parameters which describe the above mentioned three effects is much needed for improving parcel models. The driving forces responsible for the typical features of the free energy profiles are generally valid for a wide range of liquid/vapor,liquid/liquid and liquid/solid surfaces. They presumably depend only weakly on the chemical nature of the SOAs, which suggest that developing such a parametrization is feasible.

5 Data availability

A set PLUMED input files and starting configurations are available upon request.

Video supplement. Video supplements of sample steered MD simulations are available at ...

Appendix A: Structural analysis

A1 Intrinsic surface analysis and intrinsic density profiles

We label molecules of forming the organic/water interface in a time resolved manner using the ITIM method (Sega et al., 2018). ITIM selects interfacial molecules by solely geometric criteria, and is thus faster than the self-consistent technique (Chacón and Tarazona, 2003) often used for similar analysis, with essentially no loss in accuracy. (**?**) The ITIM method uses a probe sphere with a radius similar to the Lennard-Jones σ parameter of the surface atoms, in our case a value of $r = 0.2$ nm is used. The probe sphere is moved along a grid of testlines (ngrid=200 in our analysis) perpendicular to the macroscopic plane of the interface. Once the probe sphere touches a an atom, the molecule to which it belongs to is labeled as interfacial. This step uses a simple Pythagorean approach to determine whether a molecules is hit by the probe sphere. The list of surface molecules allows for the reconstruction of the intrinsic density profiles:

$$\rho(z) = \frac{1}{A}\left\langle \sum_i \delta_i(z - z_i) + \xi(x_i, y_i) \right\rangle, \tag{A1}$$

where A is the macroscopic surface area of the interface, x_i,y_i and z_i are the Cartesian coordinates of the atoms constituting the system and z is the position with respect to the local interface. $\xi(x_i, y_i) \sim kT/q^2$ is the capillary wave mode spectrum, with q being the wave vector. In simple terms intrinsic density profiles are anchored to the first molecular layer of one of the condensed phase (the aqueous phase in our case), instead of being calculated along an external grid, thus they are able to resolve the near-surface fine structure of the density profiles which are otherwise washed away by capillary wave fluctuations. Intrinsic number density profile are used to compare free energy profiles with in a qualitative manner. On the other hand mole

fraction profiles along the reaction coordinate are also estimated from the intrinsic number density profiles of the water and organic molecules. The ITIM algorithm in particular allows for the separation of the surface molecules from those belonging to the bulk, and thus repetition of the algorithm on the remaining bulk phase molecules can yield consecutive subsurface layers, which is used for determining orientational profiles.

Appendix B: Thermodynamic Analysis

The free energy profiles were decomposed into enthalpic and various entropic contributions in order to understand the effects responsible for the features observed in the in the free energy profiles

B1 Enthalpy and hydrogen bonding

On the canonical ensemble enthalpy change of a process can be approximated by the internal energy change ($p\Delta V = 0$). The internal energy profile of the transfer processes is estimated as the sum of the interaction energy between the pulled water molecule and the organic and water molecules weighted by the local mole fraction of the above two.

$$\Delta E_i(s) = x_s^l(s) * E_i(p,s) + x_w^l(s) * E_i(p,w), \tag{B1}$$

with $E_i(p,s)$ and $E_i(p,w)$ being the interaction energy between the pulled molecule and the solutes/water, calculated as the sum of short-term Coulombic and Lennard-Jones interactions (example values are listed in Table **??**). $x_s^l(s)$ and $x_w^l(s)$ are local mole fraction profiles of the water and the organics. Local mole fraction profiles are calculated from the number of water and organic molecules found within 1 nm of the pulled molecule. The cutoff distance of 1 nm corresponds to the cutoff used in the simulations for short range interactions. This calculation is only plausible because solute/water interactions in the OPLS and TIP4P forcefields were parametrized partially on quantum chemical calculations, thus individual interaction energies are physically meaningful. Equation B1 is evaluated for all realizations and averaged to yield the final profiles. Enthalpy profiles of selected realizations are shown in

Table B1. Coulombic and Lennard-Jones contributions of the interaction energies in selected realisations

	R1		R2		R3	
Type	$200K$	$300K$	$200K$	$300K$	$200K$	$300K$
LJ(p,s)	0.2 (0.1)	-0.3 (0.07)	-0.43 (0.2)	-0.2 (0.02)	-0.09 (0.02)	-0.09 (0.06)
Coulomb(p,s)	-5.7 (1.3)	-3.4 (1.1)	-5.4 (2.1)	-3.7 (1.2)	-6.8 (3)	-3.8 (1.3)
LJ(p,w)	14.4 (1.9)	11.3 (1.5)	15.1 (2.2)	11.1 (1.4)	14.2 (2.1)	10.9 (1.4)
Coulomb(p,w)	-74.5 (10.5)	-66.5 (8.5)	-75.7 (10.4)	-66.4 (8.2)	-71.8 (10.2)	-65.6 (1.0)

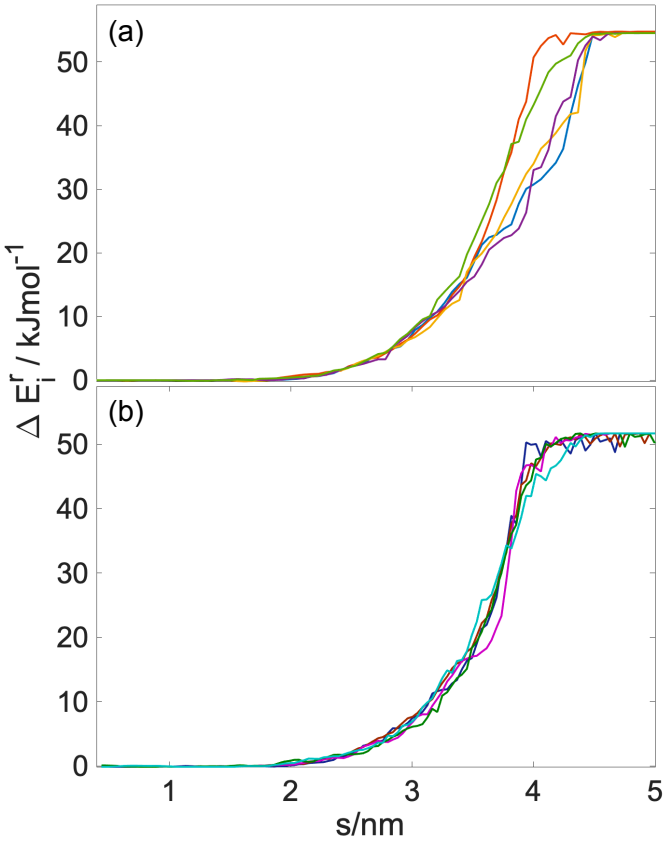

Figure B1. Enthalpy profiles of selected realisations, a) 200 K, b) 300 K.

The formation of hydrogen bonds is a major energetic driving force of the water uptake process. Figure B2 shows the number of total hydrogen bonds along the direction of the collective variable. A notable feature is that total hydrogen-bond numbers are not reduced at the organic/water interface.

The total interaction energy (enthalpy) change accompanying the water uptake process is comparable with the energy gain of the formation of on average 3 hydrogen bonds by the pulled molecule, if the energy of a single hydrogen bond is ~ 20 kJ mol^{-1}().

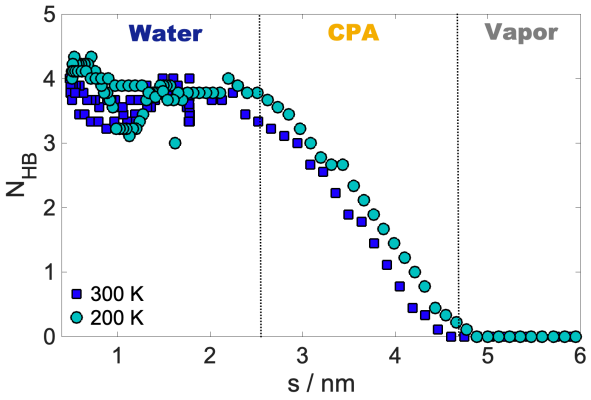

Figure B2. The number of hydrogen bonds formed by the pulled molecules along the reaction coordinate

B2 Entropy

B2.1 Interfacial entropy

Interfacial entropy accompanying any molecular transfer across phase boundaries can be calculated using the following formula from statistical thermodynamics (Ward, 2002):

$$\frac{\Delta S_{IF}}{k} = 4\left(1-\frac{T_L}{T_V}\right)+\left(\frac{1}{T_L}-\frac{1}{T_V}\right)\sum_{l=1}^{3}\left(\frac{\hbar\omega_l}{2k}+\frac{\hbar\omega_l/k}{exp(\hbar\omega_l/kT_V)-1}\right)+ \\ +\frac{v_L^{sat}}{kT_L}[P_V-P_{sat}(T_L)]+ln\left[\left(\frac{T_L}{T_V}\right)^4\left[\frac{P_{sat}(T_L)}{P_V}\right]+ln\left[\frac{q_{vib}(T_V)}{q_{vib}(T_L)}\right]\right], \quad \text{(B2)}$$

where T_V and T_L are the temperatures of the vapor and the liquid phase, P_{sat} and P_V are the saturated and the actual vapor pressure, v_L is the specific volume of the liquid phase ω_i are the vibrational frequencies and q_{vib} is the vibrational partition function. Figure B3 shows the modeled $T\Delta S_{IF}$ profiles at the two simulated temperatures, the values corresponding to the vapor pressures in the simulation box are highlighted with asterisks. The vapor pressure in the simulation box is estimated assuming the presence of the pulled molecule only in the vapor phase, using the universal gas law.

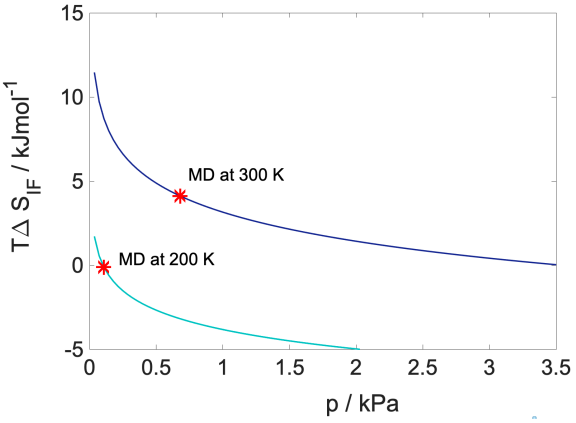

Figure B3. Modeled interfacial entropies at the simulated temperatures

B2.2 Conformational entropy

The conformational entropy profile is estimated as:

$$S_{conf} = -k_B \sum_i x_i(s) ln(x_i(s)), \tag{B3}$$

where $x_i(s)$ denotes mole fraction profiles of the components of the systems, with s being the reaction coordinate used in the steered MD simulations.

B2.3 Configurational entropy

We calculate configurational entropy according to Schlitter's formula(Baron et al., 2006), thus based on the covariance matrix ((D)) of the atomic coordinates between two distinct groups of atoms, one being the pulled molecule and the other is either the ensemble of the solutes or waters constituting the bulk phase.

$$S_{config} = \frac{k_B}{2} \ln \det \left(1 + \frac{k_B T e^2}{\hbar} \mathbf{D}\right), \tag{B4}$$

where $\hbar$ is the Planck's constant divided by 2π Two different contributions of the configurational entropy are considered i) between the pulled molecule and the solutes and between the pulled molecule and the solvents. In similar manner as for the internal energy, the weighted sum of these two yields the configurational entropy profile along the reaction coordinate (s), with the weights being the local mole fractions of water and the solutes, whose calculation is described in the previous section.

B2.4 Orientational entropy

We propose an equation which can serve as a qualitative descriptor of the entropy related to the orientation of the molecules based on equations for translational (Bhandary et al., 2016) and translational-orientation entropy terms. (Piaggi and Parrinello,

2018). With a simple exchange of the radial distribution function in (Bhandary et al., 2016) with the angular distribution function ($g(\theta)$) of the angle (θ) between the dipole vector of the water molecules and the surface normal axis, we obtain an expression for orientational entropy:

$$S_{or} = -2\pi k_B \int \left[g(\theta) ln g(\theta) - g(\theta) + 1\right] sin\theta d\theta \tag{B5}$$

This expression is evaluated for angular distribution functions calculated in the first two molecular layers and the bulk of the aqueous phase, to highlight the effect of increased molecular order on the free energy profiles. The separation of interfacial water molecules and those constituting the second layer is performed by two consecutive repetitions of the ITIM algorithm, using the output bulk phase of the first one as input for the second one.

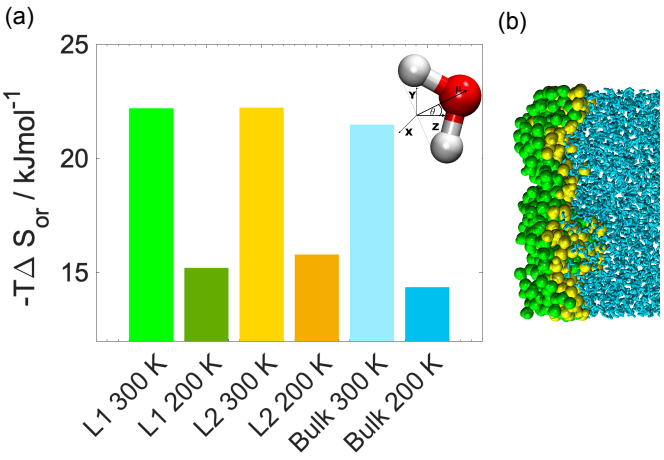

Figure B4. a) Orientational entropies in the first and second molecular layers and the bulk phase for both simulated temperatures. Inset: the definition of the θ angle. b) Snapshot from a 300 K realisation showing the first two molecular layers of the aqueous phase in green (L1) and yellow (L2).

At both temperatures the bulk phase orientational entropy is higher ($-T\Delta S$ is lower) then in the first two layers due to stronger ordering in the first two interfacial layers(Figure B4). We note that equation B5 cannot completely describe the entropy loss due to preferential ordering of the water molecules at the interface since due to its point group symmetry (C_{2v}), the orientation of water molecules with respect to an external vector or plane cannot be described with a single angle, instead the joint distribution of two angles is necessary. The development of an adapted expression of the orientational entropy of such cases is however out of the scope of this study. To complete the description of orientational differences between the surface and the bulk of the aqueous phase, we calculate joint distributions of angles cosθ' and ϕ, which are chosen to fully describe the orientation of water molecules with respect to the normal vector of the macroscopic surface(Bartok-Partay et al., 2008), in the first two molecular layers and the bulk. θ' and ϕ are defined in a Cartesian frame centered on the water molecules, the **z** axis points from the water oxygen towards the midpoint of the segment connecting the hydrogen atoms, the **y** axis is parallel to that segment, and the **x** axis is perpendicular to both **z** and **y**. θ' is the angle between the macroscopic surface normal vector

(**Z**) and the molecule centered **z** axis, and ϕ is the angle between the **x** axis and the projection of the surface normal vector to the **x**,**y** plane.

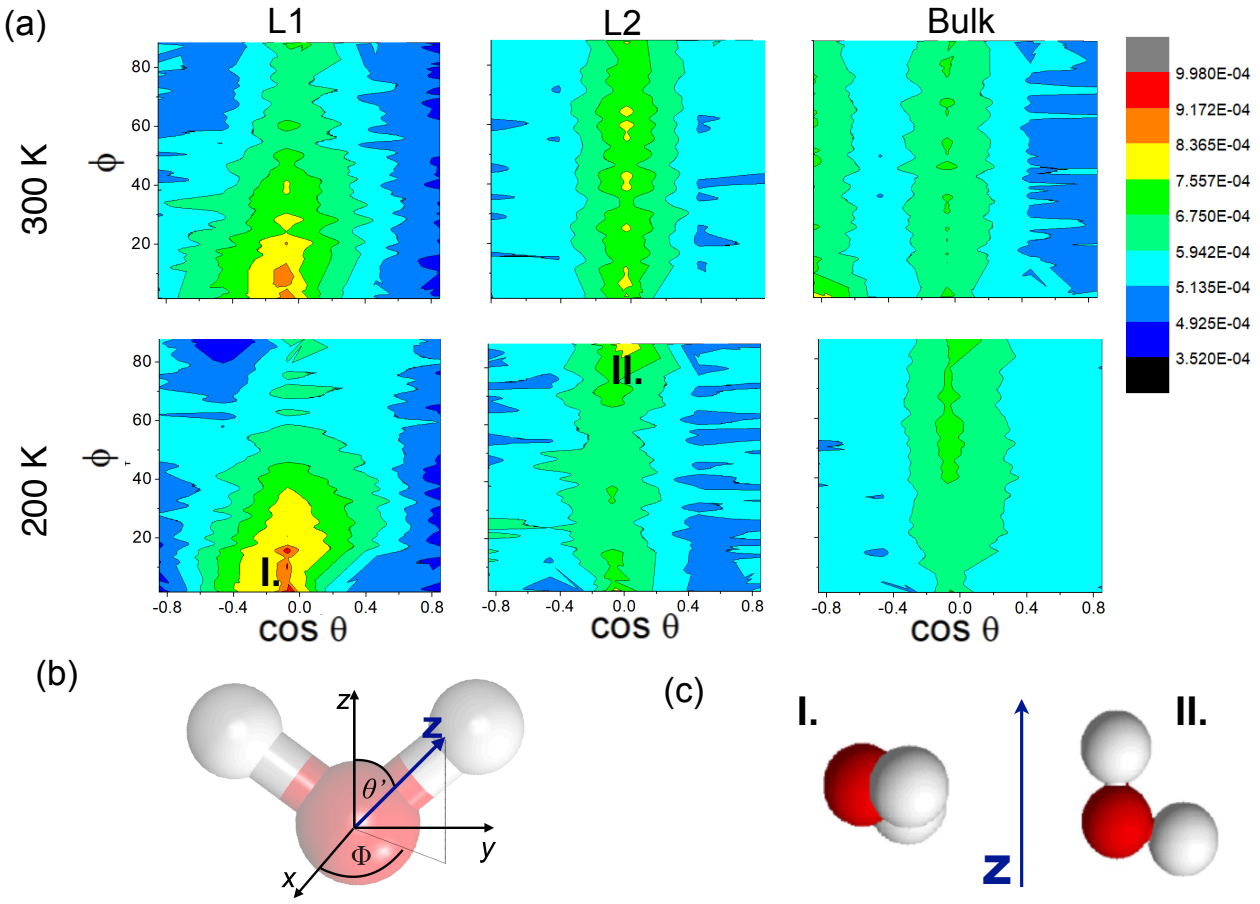

Figure B5. (a) Orientational maps of the water molecules in the first (L1), second (L2) molecular layer and the bulk phase. (b) The definition of θ' and ϕ in the Cartesian frame centered on a water. (c) Examples of the two main orientations.

Figure B5 shows orientational maps in the first two molecular layers and the bulk of the aqueous phase. In the first layer water molecules show a very strong preference to be aligned with dipole vectors parallel to the surface or slightly tilted towards the bulk aqueous phase, orientation I. in Figure B5 a) and c). In another distinguished orientation, which appears in the first and second layer at 300 K and the second layer at 200 K, one O-H bond points in the direction of the surface normal vector and the other slightly inwards to the bulk aqueous phase. Orientational preferences diminish progressively when moving towards the bulk phase, indicating the decrease of orientational order and thus a increase in orientational entropy. It is a remarkable difference between our system and aqueous interfaces of hydrophobic organic compounds (dichloromethane and dichloroethane) studied previously (Hantal et al., 2010), where preferred orientations were only found in the first molecular

layer of water in direct contact with the organic phase, that the second layer is more ordered than the bulk phase, it is due to the fact that CPA mixes more readily with water then hydrophobic organics, thus CPA molecules can penetrate into the second and third molecular layer as well into the bulk phase, and contact with the dissolved organic molecules promotes orientations that are similar to those found at the interface. We also note that the preferred orientations found of interfacial waters are universal across a large spectra of organic/water interfaces.

Author contributions. M.L.D designed and performed simulations and analysis and wrote the manuscript. S.T. and A.N. contributed to analysis, interpreted results and wrote the manuscript.

Competing interests. The authors declare no competing interests

Disclaimer. TEXT

Acknowledgements. TEXT

References

Abraham, M. J., Murtola, T., Schulz, R., Páll, S., Smith, J. C., Hess, B., and Lindahl, E.: GROMACS: High Performance Molecular Simulations through Multi-level Parallelism from Laptops to Supercomputers, SoftwareX, 1-2, 19 – 25, 2015.

Allen, W. J., Wiley, M. R., Myles, K. M., Adelman, Z. N., and Bevan, D. R.: Steered molecular dynamics identifies critical residues of the Nodamura virus B2 suppressor of RNAi, Journal of Molecular Modeling, 20, 2092, https://doi.org/10.1007/s00894-014-2092-0, https://doi.org/10.1007/s00894-014-2092-0, 2014.

Bahadur, R. and Russell, L.: Water uptake coefficients and deliquescence of NaCl nanoparticles at atmospheric relative humidities from molecular dynamics simulations, The Journal of chemical physics, 129, 094 508, https://doi.org/10.1063/1.2971040, 2008.

Baron, R., de Vries, A. H., Hünenberger, P. H., and van Gunsteren, W. F.: Configurational Entropies of Lipids in Pure and Mixed Bilayers from Atomic-Level and Coarse-Grained Molecular Dynamics Simulations, The Journal of Physical Chemistry B, 110, 15 602–15 614, https://doi.org/10.1021/jp061627s, https://doi.org/10.1021/jp061627s, pMID: 16884285, 2006.

Bartok-Partay, L., Horvai, G., and Jedlovszky, P.: Molecular level structure of the liquid/liquid interface. Molecular dynamics simulation and ITIM analysis of the water-CCl4 system, Physical chemistry chemical physics : PCCP, 10, 4754–64, https://doi.org/10.1039/b807299j, 2008.

Bhandary, D., Benková, Z., Cordeiro, M. N. D. S., and Singh, J. K.: Molecular dynamics study of wetting behavior of grafted thermo-responsive PNIPAAm brushes, Soft Matter, 12, 3093–3102, https://doi.org/10.1039/C5SM02684A, http://dx.doi.org/10.1039/C5SM02684A, 2016.

Braga, C., Muscatello, J., Lau, G., Müller, E. A., and Jackson, G.: Nonequilibrium study of the intrinsic free-energy profile across a liquid-vapour interface, The Journal of Chemical Physics, 144, 044 703, https://doi.org/10.1063/1.4940137, https://doi.org/10.1063/1.4940137, 2016.

Bussi, G., Donadio, D., and Parrinello, M.: Canonical Sampling through Velocity Rescaling, J. Chem. Phys., 126, 014 101, 2007.

Chacón, E. and Tarazona, P.: Intrinsic Profiles beyond the Capillary Wave Theory: A Monte Carlo Study, Phys. Rev. Lett., 91, 166 103, https://doi.org/10.1103/PhysRevLett.91.166103, https://link.aps.org/doi/10.1103/PhysRevLett.91.166103, 2003.

Chowdhary, J. and Ladanyi, B. M.: Surface fluctuations at the liquid-liquid interface, Phys. Rev. E, 77, 031 609, https://doi.org/10.1103/PhysRevE.77.031609, https://link.aps.org/doi/10.1103/PhysRevE.77.031609, 2008.

Clement, C. F., Kulmala, M., and Vesala, T.: Theoretical consideration on sticking probabilities, Journal of Aerosol Science, 27, 869 – 882, https://doi.org/https://doi.org/10.1016/0021-8502(96)00032-8, http://www.sciencedirect.com/science/article/pii/0021850296000328, fuchs Memorial Issue, 1996.

Darvas, M., Pojják, K., Horvai, G., and Jedlovszky, P.: Molecular dynamics simulation and identification of the truly interfacial molecules (ITIM) analysis of the liquid-vapor interface of dimethyl sulfoxide, The Journal of Chemical Physics, 132, 134 701, https://doi.org/10.1063/1.3368111, https://doi.org/10.1063/1.3368111, 2010a.

Darvas, M., Pártay, L. B., Jedlovszky, P., and Horvai, G.: Computer simulation and ITIM analysis of the surface of water–methanol mixtures containing traces of water, Journal of Molecular Liquids, 153, 88 – 93, https://doi.org/https://doi.org/10.1016/j.molliq.2009.06.004, http://www.sciencedirect.com/science/article/pii/S0167732209001287, uNDERSTANDING SOLVATION from LIQUID to SUPERCRITICAL CONDITIONS, 2010b.

Darvas, M., Gilányi, T., and Jedlovszky, P.: Competitive Adsorption of Surfactants and Polymers at the Free Water Surface. A Computer Simulation Study of the Sodium Dodecyl Sulfate-Poly(ethylene oxide) System, The Journal of Physical Chemistry B, 115, 933–944, https://doi.org/10.1021/jp110270c, https://doi.org/10.1021/jp110270c, pMID: 21250730, 2011a.

Darvas, M., Jorge, M., D. S. Cordeiro, M. N., and Jedlovszky, P.: Solvation Free Energy Profile of the SCN– Ion across the Water–1,2-Dichloroethane Liquid/Liquid Interface. A Computer Simulation Study, The Journal of Physical Chemistry C, 115, 11 140–11 146, https://doi.org/10.1021/jp2018605, https://doi.org/10.1021/jp2018605, 2011b.

Darvas, M., Jorge, M., Cordeiro, M. N. D. S., Kantorovich, S. S., Sega, M., and Jedlovszky, P.: Calculation of the Intrinsic Solvation Free Energy Profile of an Ionic Penetrant Across a Liquid–Liquid Interface with Computer Simulations, The Journal of Physical Chemistry B, 117, 16 148–16 156, https://doi.org/10.1021/jp404699t, https://doi.org/10.1021/jp404699t, pMID: 24175995, 2013.

Davidovits, P., Worsnop, D., Jayne, J., Kolb, C., Winkler, P., Vrtala, A., Wagner, P., Kulmala, M., Lehtinen, K., Vesala, T., et al.: Mass accommodation coefficient of water vapor on liquid water, 2004.

Davies, J., Miles, R., Haddrell, A., and Reid, J.: Influence of organic films on the evaporation and condensation of water in aerosol, Proceedings of the National Academy of Sciences of the United States of America, https://doi.org/10.1073/pnas.1305277110, 2013.

Diveky, M. E., Roy, S., Cremer, J. W., David, G., and Signorell, R.: Assessing relative humidity dependent photoacoustics to retrieve mass accommodation coefficients of single optically trapped aerosol particles, Phys. Chem. Chem. Phys., 21, 4721–4731, https://doi.org/10.1039/C8CP06980H, http://dx.doi.org/10.1039/C8CP06980H, 2019.

Ergin, G. and Takahama, S.: Carbon Density Is an Indicator of Mass Accommodation Coefficient of Water on Organic-Coated Water Surface, The Journal of Physical Chemistry A, 120, 2885–2893, https://doi.org/10.1021/acs.jpca.6b01748, https://doi.org/10.1021/acs.jpca.6b01748, pMID: 27089481, 2016.

Essmann, U., Perera, L., Berkowitz, M. L., Darden, T., Lee, H., and Pedersen, L. G.: A Smooth Particle Mesh Ewald Method, J. Chem. Phys., 103, 8577–8593, 1995.

Facchini, M. C., Mircea, M., Fuzzi, S., and Charlson, R. J.: Cloud albedo enhancement by surface-active organic solutes in growing droplets, Nature, 401, 257–259, https://doi.org/10.1038/45758, https://doi.org/10.1038/45758, 1999.

Fuzzi, S., Andreae, M. O., Huebert, B. J., Kulmala, M., Bond, T. C., Boy, M., Doherty, S. J., Guenther, A., Kanakidou, M., Kawamura, K., Kerminen, V.-M., Lohmann, U., Russell, L. M., and Pöschl, U.: Critical assessment of the current state of scientific knowledge, terminology, and research needs concerning the role of organic aerosols in the atmosphere, climate, and global change, Atmospheric Chemistry and Physics, 6, 2017–2038, https://doi.org/10.5194/acp-6-2017-2006, https://www.atmos-chem-phys.net/6/2017/2006/, 2006.

Gorkowski, K., Donahue, N. M., and Sullivan, R. C.: Emulsified and liquid–liquid phase-separated states of α-pinene secondary organic aerosol determined using aerosol optical tweezers, Environmental Science & Technology, 51, 12 154–12 163, 2017.

Hantal, G., Darvas, M., Pártay, L. B., Horvai, G., and Jedlovszky, P.: Molecular level properties of the free water surface and different organic liquid/water interfaces, as seen from ITIM analysis of computer simulation results, Journal of Physics: Condensed Matter, 22, 284 112, https://doi.org/10.1088/0953-8984/22/28/284112, https://doi.org/10.1088%2F0953-8984%2F22%2F28%2F284112, 2010.

Hummer, G. and Szabo, A.: Free energy reconstruction from nonequilibrium single-molecule pulling experiments, Proceedings of the National Academy of Sciences, 98, 3658–3661, https://doi.org/10.1073/pnas.071034098, https://www.pnas.org/content/98/7/3658, 2001.

Hyvärinen, A.-P., Lihavainen, H., Gaman, A., Vairila, L., Ojala, H., Kulmala, M., and Viisanen, Y.: Surface Tensions and Densities of Oxalic, Malonic, Succinic, Maleic, Malic, and cis-Pinonic Acids, Journal of Chemical & Engineering Data, 51, 255–260, https://doi.org/10.1021/je050366x, https://doi.org/10.1021/je050366x, 2006.

IPCC, .: Summary for policymakers.

Johansson, S. M., Lovrić, J., Kong, X., Thomson, E. S., Hallquist, M., and Pettersson, J. B. C.: Experimental and Computational Study of Molecular Water Interactions with Condensed Nopinone Surfaces Under Atmospherically Relevant Conditions, The Journal of Physical Chemistry A, 0, null, https://doi.org/10.1021/acs.jpca.9b10970, https://doi.org/10.1021/acs.jpca.9b10970, pMID: 32281376, 2020.

Jorge, M., Hantal, G., Jedlovszky, P., and Cordeiro, M. N. D. S.: A Critical Assessment of Methods for the Intrinsic Analysis of Liquid Interfaces: 2. Density Profiles, The Journal of Physical Chemistry C, 114, 18 656–18 663, https://doi.org/10.1021/jp107378s, https://doi.org/10.1021/jp107378s, 2010.

Jorgensen, W. L. and Tirado-Rives, J.: The OPLS [Optimized Potentials for Liquid Simulations] Potential Functions for Proteins, Energy Minimizations for Crystals of Cyclic Peptides and Crambin, J. Am. Chem. Soc., 110, 1657–1666, 1988.

Jorgensen, W. L., Chandrasekhar, J., Madura, J. D., Impey, R. W., and Klein, M. L.: Comparison of Simple Potential Functions for Simulating Liquid Water, J. Chem. Phys., 79, 926–935, 1983.

Kertész, J., Darvas, M., Jedlovszky, P., and Horvai, G.: Reprint of "Role of the fluidity of a liquid phase in determining the surface properties of the opposite phase", Journal of Molecular Liquids, 189, 122 – 128, https://doi.org/https://doi.org/10.1016/j.molliq.2013.06.009, http://www.sciencedirect.com/science/article/pii/S0167732213002110, fluid phase associations, 2014.

Krieger, U. K., Marcolli, C., and Reid, J. P.: Exploring the complexity of aerosol particle properties and processes using single particle techniques, Chem. Soc. Rev., 41, 6631–6662, https://doi.org/10.1039/C2CS35082C, http://dx.doi.org/10.1039/C2CS35082C, 2012.

Li, Y. Q., Davidovits, P., Kolb, C. E., and Worsnop, D. R.: Mass and Thermal Accommodation Coefficients of H2O(g) on Liquid Water as a Function of Temperature, The Journal of Physical Chemistry A, 105, 10 627–10 634, https://doi.org/10.1021/jp012758q, https://doi.org/10.1021/jp012758q, 2001.

Lienhard, D. M., Huisman, A. J., Krieger, U. K., Rudich, Y., Marcolli, C., Luo, B. P., Bones, D. L., Reid, J. P., Lambe, A. T., Canagaratna, M. R., Davidovits, P., Onasch, T. B., Worsnop, D. R., Steimer, S. S., Koop, T., and Peter, T.: Viscous organic aerosol particles in the upper troposphere: diffusivity-controlled water uptake and ice nucleation?, Atmospheric Chemistry and Physics, 15, 13 599–13 613, https://doi.org/10.5194/acp-15-13599-2015, https://www.atmos-chem-phys.net/15/13599/2015/, 2015.

Liu, P., Song, M., Zhao, T., Gunthe, S. S., Ham, S., He, Y., Qin, Y. M., Gong, Z., Amorim, J. C., Bertram, A. K., and Martin, S. T.: Resolving the mechanisms of hygroscopic growth and cloud condensation nuclei activity for organic particulate matter, Nature Communications, 9, 4076, https://doi.org/10.1038/s41467-018-06622-2, https://doi.org/10.1038/s41467-018-06622-2, 2018.

Liu, X., Day, D. A., Krechmer, J. E., Brown, W., Peng, Z., Ziemann, P. J., and Jimenez, J. L.: Direct measurements of semi-volatile organic compound dynamics show near-unity mass accommodation coefficients for diverse aerosols, Communications Chemistry, 2, 98, https://doi.org/10.1038/s42004-019-0200-x, https://doi.org/10.1038/s42004-019-0200-x, 2019.

Miles, R. E. H., Reid, J. P., and Riipinen, I.: Comparison of Approaches for Measuring the Mass Accommodation Coefficient for the Condensation of Water and Sensitivities to Uncertainties in Thermophysical Properties, The Journal of Physical Chemistry A, 116, 10 810–10 825, https://doi.org/10.1021/jp3083858, https://doi.org/10.1021/jp3083858, pMID: 23057492, 2012.

Miles, R. E. H., Davies, J. F., and Reid, J. P.: The influence of the surface composition of mixed monolayer films on the evaporation coefficient of water, Phys. Chem. Chem. Phys., 18, 19 847–19 858, https://doi.org/10.1039/C6CP03826C, http://dx.doi.org/10.1039/C6CP03826C, 2016.

Moore, R. H., Raatikainen, T., Langridge, J. M., Bahreini, R., Brock, C. A., Holloway, J. S., Lack, D. A., Middlebrook, A. M., Perring, A. E., Schwarz, J. P., et al.: CCN spectra, hygroscopicity, and droplet activation kinetics of secondary organic aerosol resulting from the 2010 Deepwater Horizon oil spill, Environmental science & technology, 46, 3093–3100, 2012.

Morales Betancourt, R. and Nenes, A.: Understanding the contributions of aerosol properties and parameterization discrepancies to droplet number variability in a global climate model, Atmospheric Chemistry and Physics, 14, 4809–4826, https://doi.org/10.5194/acp-14-4809-2014, https://www.atmos-chem-phys.net/14/4809/2014/, 2014.

Morita, A., Sugiyama, M., Kameda, H., Koda, S., and Hanson, D. R.: Mass Accommodation Coefficient of Water: Molecular Dynamics Simulation and Revised Analysis of Droplet Train/Flow Reactor Experiment, The Journal of Physical Chemistry B, 108, 9111–9120, https://doi.org/10.1021/jp030479s, 2004.

Noziere, B.: Don't forget the surface, Science, 351, 1396–1397, https://doi.org/10.1126/science.aaf3253, https://science.sciencemag.org/content/351/6280/1396, 2016.

Ovadnevaite, J., Zuend, A., Laaksonen, A., Sanchez, K. J., Roberts, G., Ceburnis, D., Decesari, S., Rinaldi, M., Hodas, N., Facchini, M. C., Seinfeld, J. H., and O'Dowd, C.: Surface tension prevails over solute effect in organic-influenced cloud droplet activation, Nature, 546, 637–641, https://doi.org/10.1038/nature22806, https://doi.org/10.1038/nature22806, 2017.

Pajunoja, A., Lambe, A. T., Hakala, J., Rastak, N., Cummings, M. J., Brogan, J. F., Hao, L., Paramonov, M., Hong, J., Prisle, N. L., Malila, J., Romakkaniemi, S., Lehtinen, K. E. J., Laaksonen, A., Kulmala, M., Massoli, P., Onasch, T. B., Donahue, N. M., Riipinen, I., Davidovits, P., Worsnop, D. R., Petäjä, T., and Virtanen, A.: Adsorptive uptake of water by semisolid secondary organic aerosols, Geophysical Research Letters, 42, 3063–3068, https://doi.org/10.1002/2015GL063142, https://agupubs.onlinelibrary.wiley.com/doi/abs/10.1002/2015GL063142, 2015.

Park, S. and Schulten, K.: Calculating potentials of mean force from steered molecular dynamics simulation, The Journal of chemical physics, 120, 5946–61, https://doi.org/10.1063/1.1651473, 2004.

Piaggi, P. M. and Parrinello, M.: Predicting polymorphism in molecular crystals using orientational entropy, Proceedings of the National Academy of Sciences, 115, 10 251–10 256, https://doi.org/10.1073/pnas.1811056115, https://www.pnas.org/content/115/41/10251, 2018.

Pojják, K., Darvas, M., Horvai, G., and Jedlovszky, P.: Properties of the Liquid-Vapor Interface of Water-Dimethyl Sulfoxide Mixtures. A Molecular Dynamics Simulation and ITIM Analysis Study, The Journal of Physical Chemistry C, 114, 12 207–12 220, https://doi.org/10.1021/jp101442m, https://doi.org/10.1021/jp101442m, 2010.

Prenni, A. J., Petters, M. D., Kreidenweis, S. M., DeMott, P. J., and Ziemann, P. J.: Cloud droplet activation of secondary organic aerosol, Journal of Geophysical Research: Atmospheres, 112, https://doi.org/10.1029/2006JD007963, https://agupubs.onlinelibrary.wiley.com/doi/abs/10.1029/2006JD007963, 2007.

Pártay, L. B., Jedlovszky, P., Vincze, , and Horvai, G.: Properties of Free Surface of Water-Methanol Mixtures. Analysis of the Truly Interfacial Molecular Layer in Computer Simulation, The Journal of Physical Chemistry B, 112, 5428–5438, https://doi.org/10.1021/jp711547e, https://doi.org/10.1021/jp711547e, pMID: 18393551, 2008.

Raatikainen, T., Nenes, A., Seinfeld, J. H., Morales, R., Moore, R. H., Lathem, T. L., Lance, S., Padró, L. T., Lin, J. J., Cerully, K. M., Bougiatioti, A., Cozic, J., Ruehl, C. R., Chuang, P. Y., Anderson, B. E., Flagan, R. C., Jonsson, H., Mihalopoulos, N., and Smith, J. N.: Worldwide data sets constrain the water vapor uptake coefficient in cloud formation, Proceedings of the National Academy of Sciences, 110, 3760–3764, https://doi.org/10.1073/pnas.1219591110, https://www.pnas.org/content/110/10/3760, 2013.

Renbaum-Wolff, L., Song, M., Marcolli, C., Zhang, Y., Liu, P. F., Grayson, J. W., Geiger, F. M., Martin, S. T., and Bertram, A. K.: Observations and implications of liquid–liquid phase separation at high relative humidities in secondary organic material produced by α-pinene ozonolysis without inorganic salts, Atmospheric Chemistry and Physics, 16, 7969–7979, https://doi.org/10.5194/acp-16-7969-2016, https://www.atmos-chem-phys.net/16/7969/2016/, 2016.

Roy, S., Diveky, M. E., and Signorell, R.: Mass Accommodation Coefficients of Water on Organics from Complementary Photoacoustic and Light Scattering Measurements on Laser-Trapped Droplets, The Journal of Physical Chemistry C, 124, 2481–2489, https://doi.org/10.1021/acs.jpcc.9b09934, https://doi.org/10.1021/acs.jpcc.9b09934, 2020.

Ruehl, C. R., Chuang, P. Y., Nenes, A., Cappa, C. D., Kolesar, K. R., and Goldstein, A. H.: Strong evidence of surface tension reduction in microscopic aqueous droplets, Geophysical Research Letters, 39, https://doi.org/10.1029/2012GL053706, https://agupubs.onlinelibrary.wiley.com/doi/abs/10.1029/2012GL053706, 2012.

Ruehl, C. R., Davies, J. F., and Wilson, K. R.: An interfacial mechanism for cloud droplet formation on organic aerosols, Science, 351, 1447–1450, https://doi.org/10.1126/science.aad4889, https://science.sciencemag.org/content/351/6280/1447, 2016.

Saleh, R., Donahue, N. M., and Robinson, A. L.: Time Scales for Gas-Particle Partitioning Equilibration of Secondary Organic Aerosol Formed from Alpha-Pinene Ozonolysis, Environmental Science & Technology, 47, 5588–5594, https://doi.org/10.1021/es400078d, https://doi.org/10.1021/es400078d, pMID: 23647198, 2013.

Sareen, N., Schwier, A. N., Lathem, T. L., Nenes, A., and McNeill, V. F.: Surfactants from the gas phase may promote cloud droplet formation, Proceedings of the National Academy of Sciences, 110, 2723–2728, https://doi.org/10.1073/pnas.1204838110, https://www.pnas.org/content/110/8/2723, 2013.

Sega, M., Hantal, G., Fábián, B., and Jedlovszky, P.: Pytim: A python package for the interfacial analysis of molecular simulations, Journal of Computational Chemistry, 39, https://doi.org/10.1002/jcc.25384, 2018.

Shiraiwa, M. and Pöschl, U.: Mass Accommodation and Gas-Particle Partitioning in Secondary Organic Aerosols: Dependence on Diffusivity, Volatility, Particle-phase Reactions, and Penetration Depth, Atmospheric Chemistry and Physics Discussions, 2020, 1–30, https://doi.org/10.5194/acp-2020-536, https://www.atmos-chem-phys-discuss.net/acp-2020-536/, 2020.

Shiraiwa, M., Pfrang, C., Koop, T., and Pöschl, U.: Kinetic multi-layer model of gas-particle interactions in aerosols and clouds (KM-GAP): linking condensation, evaporation and chemical reactions of organics, oxidants and water, Atmospheric Chemistry and Physics, 12, 2777–2794, https://doi.org/10.5194/acp-12-2777-2012, https://www.atmos-chem-phys.net/12/2777/2012/, 2012.

Shiraiwa, M., Zuend, A., Bertram, A. K., and Seinfeld, J. H.: Gas–particle partitioning of atmospheric aerosols: interplay of physical state, non-ideal mixing and morphology, Phys. Chem. Chem. Phys., 15, 11 441–11 453, https://doi.org/10.1039/C3CP51595H, http://dx.doi.org/10.1039/C3CP51595H, 2013.

Song, M., Marcolli, C., Krieger, U. K., Zuend, A., and Peter, T.: Liquid-liquid phase separation in aerosol particles: Dependence on O:C, organic functionalities, and compositional complexity, Geophysical Research Letters, 39, https://doi.org/10.1029/2012GL052807, https://agupubs.onlinelibrary.wiley.com/doi/abs/10.1029/2012GL052807, 2012.

Song, M., Liu, P., Martin, S. T., and Bertram, A. K.: Liquid–liquid phase separation in particles containing secondary organic material free of inorganic salts, Atmospheric Chemistry and Physics, 17, 11 261–11 271, https://doi.org/10.5194/acp-17-11261-2017, https://www.atmos-chem-phys.net/17/11261/2017/, 2017.

Takahama, S. and Russell, L. M.: A molecular dynamics study of water mass accommodation on condensed phase water coated by fatty acid monolayers, Journal of Geophysical Research: Atmospheres, 116, https://doi.org/10.1029/2010JD014842, https://agupubs.onlinelibrary.wiley.com/doi/abs/10.1029/2010JD014842, 2011.

Tribello, G. A., Bonomi, M., Branduardi, D., Camilloni, C., and Bussi, G.: PLUMED 2: New Feathers for an Old Bird, Computer Physics Communications, 185, 604 – 613, 2014.

Vieceli, J., Roeselová, M., Potter, N., Dang, L. X., Garrett, B. C., and Tobias, D. J.: Molecular Dynamics Simulations of Atmospheric Oxidants at the Air-Water Interface: Solvation and Accommodation of OH and O3, The Journal of Physical Chemistry B, 109, 15 876–15 892, https://doi.org/10.1021/jp051361+, https://doi.org/10.1021/jp051361+, pMID: 16853017, 2005.

Voigtländer, J., Stratmann, F., Niedermeier, D., Wex, H., and Kiselev, A.: Mass accommodation coefficient of water: A combined computational fluid dynamics and experimental data analysis, Journal of Geophysical Research: Atmospheres, 112, https://doi.org/10.1029/2007JD008604, https://agupubs.onlinelibrary.wiley.com/doi/abs/10.1029/2007JD008604, 2007.

von Domaros, M., Lakey, P. S. J., Shiraiwa, M., and Tobias, D. J.: Multiscale Modeling of Human Skin Oil-Induced Indoor Air Chemistry: Combining Kinetic Models and Molecular Dynamics, The Journal of Physical Chemistry B, 124, 3836–3843, https://doi.org/10.1021/acs.jpcb.0c02818, https://doi.org/10.1021/acs.jpcb.0c02818, pMID: 32290653, 2020.

Ward, C.: Liquid-Vapour Phase Change Rates and Interfacial Entropy Production, Journal of Non-Equilibrium Thermodynamics, 27, 289–303, https://doi.org/10.1515/JNETDY.2002.017, 2002.

Zientara, M., Jakubczyk, D., Kolwas, K., and Kolwas, M.: Temperature Dependence of the Evaporation Coefficient of Water in Air and Nitrogen under Atmospheric Pressure: Study in Water Droplets, The Journal of Physical Chemistry A, 112, 5152–5158, https://doi.org/10.1021/jp7114324, https://doi.org/10.1021/jp7114324, pMID: 18491849, 2008.